國 立 交 通 大 學

電信工程研究所

碩士論文

於多用戶多輸入多輸出系統中
利用差動量化降低通道回饋量

CSI Feedback Reduction Based on Differential Quantization in Multi-User MIMO Systems

研 究 生：鄭佳旻　　Student: Chia-Min Cheng

指導教授：李大嵩 博士　　Advisor: Dr. Ta-Sung Lee

吳卓諭 博士　　Dr. Jwo-Yuh Wu

中 華 民 國 九 十 九 年 七 月

於多用戶多輸入多輸出系統中利用差動量化降低通道回饋量

CSI Feedback Reduction Based on Differential Quantization in Multi-User MIMO Systems

研 究 生：鄭佳旻　　Student: Chia-Min Cheng

指導教授：李大嵩 博士　　Advisor: Dr. Ta-Sung Lee

吳卓諭 博士　　Dr. Jwo-Yuh Wu

國立交通大學

電信工程研究所

碩士論文

A Thesis
Submitted to Institute of Communication Engineering
College of Electrical and Computer Engineering
National Chiao Tung University
in Partial Fulfillment of the Requirements
for the Degree of
Master of Science
in
Communication Engineering
July 2010
Hsinchu, Taiwan, Republic of China

中 華 民 國 九 十 九 年 七 月

於多用戶多輸入多輸出系統中利用差動量化降低通道回饋量

學生：鄭佳旻　　　　　　　　　　指導教授：李大嵩 博士

吳卓諭 博士

國立交通大學電信工程研究所

摘要

現代無線通訊系統中，有限回饋是近幾年備受關注的關鍵技術之一。在有限的回饋頻寬之下，如何有效量化通道資訊是系統設計的重要議題。在本篇論文中，吾人著重在基於不影響系統效能或甚至提昇系統效能的前提下降低通道回饋量。吾人提出兩種方法：第一，針對回傳通道狀態資訊，吾人提出向量差動量化。第二；對於空間相關性矩陣的回傳，吾人提出對角向量量化向量。差動量化在接收端引進預測性向量量化技術，進而利用通道的時間相關性壓縮通道回饋量；對角向量量化則主要是利用空間上的相關性來達到減少量化位元數。模擬結果顯示吾人提出的方法能較現有方法達到更好的性能表現。

CSI Feedback Reduction Based on Differential Quantization in Multi-User MIMO Systems

Student: Chia-Min Cheng Advisor: Dr. Ta-Sung Lee

Dr. Jwo-Yuh Wu

Institute of Communication Engineering

National Chiao Tung University

Abstract

Limited feedback techniques have drawn attention for many years and emerged as one of the key techniques in modern wireless communication systems. Under the finite-rate feedback link environment, the issue of how to quantize channel information efficiently becomes important for system design. In this thesis, we focus on reducing the required feedback rate while maintaining or even enhancing the performance of the overall system. We propose two methods: one is differential vector quantization (VQ) for channel state information (CSI) feedback, and the other is diagonal-wise full VQ for spatial correlation matrix feedback. The proposed differential VQ introduces Predictive Vector Quantization (PVQ) in the receiver end to compress the CSI by exploiting the temporal correlation of the channel. The diagonal-wise full VQ mainly exploits the spatial correlation of the channel to reduce the feedback quantization bits. Simulation results indicate that both methods can achieve a higher SINR and a smaller MSE compared to the existing schemes.

Acknowledgement

I am heartily thankful to my advisors, Dr. Ta-Sung Lee and Dr. Jwo-Yuh Wu, whose encouragement, guidance and support from the initial to the final level enabled me to develop an understanding of the subject. I learned a lot from their positive attitude in many areas. I also offer my regards and blessings to all members in the Communication System Design and Signal Processing (CSDSP) Lab. Last but not least, I would like to show my sincere thanks to my family for their invaluable love and support.

Table of Contents

Chinese Abstract I

English Abstract II

Table of Contents IV

List of Figures VI

List of Tables... VIII

Acronym Glossary X

Notations XI

Chapter 1 Introduction.. 1

Chapter 2 System Model 4

2.1 Limited Feedback in Multiuser MIMO Systems 5

2.2 Precoding Scheme...7

2.3 Correlated Channel Model 8

2.4 Quantization Criterion and Codebook Construction in LTE Release 8.........10

2.5 Summary 13

Chapter 3 Reduced CSI Feedback Based on Differential Qunatizaion... 14

3.1 Motivation...15

3.2 Proposed Differential Quantization Method 16

3.2.1 Incorporation of Predictor...19

3.2.2 Design of Differential VQ Codebook 20

3.2.2 Initial Full CSI and Error Accumulation....23
3.3 Computer Simulations....25
3.3.1 Simulations in Time Domain CSI Feedback....26
3.3.2 Extension to MIMO OFDM system....31
3.4 Summary....37
Chapter 4 Discussion of Different Feedback Overheads and Spatial Correlation Matrix Feedback....38
4.1 Different Feedback Overheads in Multi-user Systems....39
4.1.1 Simulation Demonstration....39
4.1.2 Geometric Interpretations....41
4.1.3 Discussions of Interferences and Precoding Gain....43
4.1.4 Conclusions....45
4.2 Proposed Diagonal-wise Vector Quantization for Spatial Correlation Matrix Feedback....46
4.2.1 Correlated Channel Model [28]....47
4.2.2 Existing Solution: Entry-wise Differential Scalar Quantization [27]....49
4.2.3 Proposed Diagonal-wise Full Vector Quantization....50
4.2.4 Comparisons Between Entry-wise Differential SQ and Proposed Diagonal-wise Full VQ....52
4.2.5 Computer Simulations....53
4.3 Summary....64
Chapter 5 Conclusion....65
Bibliography....67

List of Figures

Fig. 2-1 Limited feedback multi-user MIMO system......6

Fig. 2-2 Jakes' fading simulator......9

Fig. 2-3 Autocorrelation of Jakes' simulator under $M = 16$ 9

Fig. 2-4 Full vector quantization 10

Fig. 3-1 Comparison of DPCM and Full Scalar Quantization......15

Fig. 3-2 Limited feedback system with proposed differential VQ scheme 17

Fig. 3-3 Block diagram of PVQ system at receiver......17

Fig. 3-4 Mathematical expression of PVQ system at receiver 18

Fig. 3-5 Block diagram of PVQ system at transmitter 18

Fig. 3-6 Mathematical expression of PVQ system at transmitter......18

Fig. 3-7 GLA training process [9, 10]......21

Fig. 3-8 Two-step codebook training......22

Fig. 3-9 SINR under different number of initial full scalar quantization bits 24

Fig. 3-10 Error Accumulation......24

Fig. 3-11 Definition of Parameters 25

Fig. 3-12 Differential vector quantization vs. Full vector quantization......29

Fig. 3-13 Differential vector quantization under different $N\ (T_f)$ 29

Fig. 3-14 Differential vector quantization under different velocities 30

Fig. 3-15 LTE resource grid......31

Fig. 3-16 Differential vector quantization vs. Full vector quantization......35

Fig. 3-17 Differential vector quantization under different $N\ (T_f)$ 35

Fig. 3-18 Differential vector quantization under different velocities 36

Fig. 4-1 Simulation demonstration of different feedback overheads for different users 40

Fig. 4-2 Geometric representation for two users case 41

Fig. 4-3 Geometric representation of interference..43

Fig. 4-4 Geometric representation of precoding gain..44

Fig. 4-5 Angle parameters in MIMO channel model [14]...48

Fig. 4-6 Column wise vector quantization...50

Fig. 4-7 Diagonal-wise vector quantization..50

Fig. 4-8 Reducing the feedback frequency 51

Fig. 4-9 Different number of quantization bits for Diagonal-wise full VQ....................62

Fig. 4-10 Channel variation for high and low velocities 62

Fig. 4-11 Comparisons of the results with time-varying and time-invarying channel ...63

List of Tables

Table 2-1 4-bit Codebook Construction [25] 12

Table 3-1 Simulation Parameters 26

Table 3-2 Codebook for v = 3 km/hr..27

Table 3-3 Codebook for v = 5 km/hr..27

Table 3-4 Codebook for v = 8 km/hr..27

Table 3-5 Codebook for v = 10 km/hr..28

Table 3-6 Codebook for v = 15 km/hr..28

Table 3-7 Simulation Parameters 32

Table 3-8 Codebook for v = 3 km/hr..33

Table 3-9 Codebook for v = 5 km/hr..33

Table 3-10 Codebook for v = 8 km/hr..33

Table 3-11 Codebook for v = 10 km/hr..34

Table 3-12 Codebook for v = 15 km/hr..34

Table 4-1 Two cases in simulation 39

Table 4-2 Simulation Parameters 40

Table 4-3 Definitions of parameters..41

Table 4-4 Parameter definitions 47

Table 4-5 Values of Δ_k [30]..48

Table 4-6 Comparisons of diagonal-wise full VQ and enty-wise differential SQ 52

Table 4-7 Simulation parameters..54

Table 4-8 Codebooks for third diagonal (1×1 vector) under time-invariant channel environment 55

Table 4-9 Codebooks for secondary diagonal (2×1 vector) under time-invariant channel environment..55

Table 4-10 Codebooks for main diagonal (3×1 vector) under time-invariant channel environment 57

Table 4-11 Codebooks for third diagonal (1×1 vector) under time-varying channel environment 58

Table 4-12 Codebooks for secondary diagonal (2×1 vector) under time-varying channel environment...58

Table 4-13 Codebooks for main diagonal (3×1 vector) under time-varying channel environment 60

Acronym Glossary

CSI	channel state information
PVQ	predictive vector quantization
SINR	signal to interference and noise ratio
MIMO	multiple-input multiple-output
MISO	multiple-input single-output
VQ	vector quantization
SQ	scalar quantization
MSE	mean squared error
ZF	zero-forcing
GLA	generalized Lloyd algorithm

Notations

P	total power constraint for single user
M	number of transmit antennas
K	number of mobile users
n_k	complex Gaussian noise for the user k
σ^2	variance of complex Gaussian noise
$\mathbf{h}_n$	channel vector at the n th time instant
$\overline{\mathbf{h}}_n$	quantized channel vector at the n th time instant
$\mathbf{c}_l$	codeword with index l
$\mathbf{e}_n$	differential CSI at the n th time instant
$\overline{\mathbf{e}}_n$	quantized differential CSI at the n th time index
$\mathbf{v}_i$	beamforming vector for the user i
R_d	number of quantization bits per channel vector for full CSI
R_f	number of quantization bits per channel vector for differential CSI
R_{avg}	average number of quantization bits per cannel vector
α	quantization angular error
β	angle between $\overline{\mathbf{h}}_i$ and $\mathbf{v}_i$ for the user i

Chapter 1

Introduction

Multiple-input multiple-output (MIMO) technologies have demonstrated the potential to significantly enhance the performance of wireless communications. In the case of multi-user MIMO systems, simultaneous transmissions of multiple user signals can be supported by space-division multiple access to provide a substantial gain in system throughput. Nevertheless multiple access introduces interferences in the system. Designing transmit vectors while considering the interference of other users is quite challenging. In this case, CSI at the transmitter enables the communication system to exploit the channel information and avoid interference. The precoders which can increase various performance gains for wireless communication [1] can be designed based on different forms of the channel information available to the transmitter [2-4]. When perfect CSI is available at the transmitter and receiver, the well-known dirty-paper coding is used to pre-cancel multiuser interference at the transmitter and hence achieves full channel capacity [5].

However, conveying perfect full CSI would impose a heavy burden on user feedback channel and the amount of feedback information increases with the number of users in service. For this reason, research on partial CSI feedback under limited feedback link has drawn much attention recently since it was proposed in [6, 7]. For limited feedback systems, issues like transmission delays, channel estimation error at the receiver, quantization error, and non-ideal feedback link can cause problems to the overall system. Many research works have investigated the utilization of limited feedback systems and tried to solve the above problems [8-14]. Some of them focus on reducing CSI feedback overhead by designing an optimum codebook or quantizing the CSI efficiently [10, 12-14] since resource is valuable under the limited feedback environments.

In this thesis, our goal is to reduce the required feedback overhead by effectively quantizing the channel information. Considering multiuser MIMO systems (each users with a single antenna), we try to quantize the CSI via vector quantization. The proposed differential vector quantization adopts the Predictive Vector Quantization (PVQ) model [15] to perform differential quantization by exploiting the temporal correlation of CSI. The proposed scheme periodically feeds back the full CSI using a large number of quantization bits while using fewer bits to quantize the remaining differential CSI. We make the average number of quantization bits smaller than that of the conventional full vector quantization. We further extend the MIMO system to a MIMO OFDM system. Instead of quantizing the time domain CSI, frequency domain CSI, or subcarrier, requires much more quantization bits since at every time instant, the number of subcarrier may be up to 2048 in LTE systems. It is impossible to feed back all the subcarriers information. Hence, only some of the subcarriers are chosen to be fed back. Although the temporal correlation of subcarriers is not as obvious as the CSI in time domain, simulations show that the proposed differential vector quantization is still effective in MIMO OFDM systems.

In addition to CSI at the transmitter end, spatial correlation matrix can also be used to modify the precoding matrix to make the precoding matrix more suitable in the current communication environments. Therefore, for the system which needs spatial correlation statistic information at the transmitter end, we propose a diagonal-wise full vector quantization scheme to quantize the matrix efficiently and thereby reducing the feedback overhead.

In this thesis, we also investigate the scenario where some users are granted a higher feedback overhead. From a geometrical point of view, we show a simple example to illustrate one user' performance changes in the case that some other users are permitted to have a higher feedback overhead.

This thesis is organized as follows. Chapter 2 describes the system model and the conventional full VQ scheme. In Chapter 3, the proposed differential vector quantization is introduced along with our codebook design method and the incorporation of predictor. And in Chapter 4, we explain users' performance under different feedback overheads and present the proposed diagonal-wise full vector quantization for spatial correlation matrix feedback. Numerical results illustrate the advantages of the proposed methods. Finally, we conclude this thesis in Chapter 5.

Chapter 2

System Model

In wireless communication environments, multiple-input multiple-output (MIMO) system provides significant increases in data throughput without additional bandwidth and transmission power [16]. There are two modes in a MIMO system, one is the open loop mode and the other is the closed loop mode. The basic idea of the closed loop mode is to use channel information to adapt the transmitted signal. If channel state information (CSI) is available at the transmitter, a precoder can be pre-designed to match the channel, and thereby offers diversity and yields a better performance. However, in limited feedback systems, it is impossible for the transmitter to know accurate and instantaneous CSI. The estimated CSI at the receiver end is quantized by a given codebook and the receiver will feed back the index of selected codeword to the transmitter.

Since limited feedback systems can only have a finite codebook size, codebook design becomes an essential issue and a difficult problem. A good codebook may reduce the feedback overhead while maintaining performance. The statistical distribution of the channel and quantization criterion must be taken into account to design a codebook. In [17], the random vector quantization (RVQ) method provides a simple way for codebook construction. Also, the problem of designing codebook is shown to be equivalent to Grassmannian line packing in [18].

In this chapter, the multiuser MIMO system with limited feedback will be introduced first. And then the linear precoding method of the system is discussed. Finally, the codebook in LTE Release V8.7.0 (2009-05) will be introduced and its construction be presented.

2.1 Limited Feedback in Multiuser MIMO Systems

The communication system with a limited feedback link requires cooperation between the transmitter and receiver. The limited feedback multiuser MIMO system is illustrated in Figure 2.1. The MIMO system has M transmit antennas and each receiver has a single antenna. The broadcast channel can be described as

$$y_i = \mathbf{h}_i^H \mathbf{s} + n_i, \qquad i = 1, \ldots, K \tag{2.1}$$

where $\mathbf{h}_1, \mathbf{h}_2, \ldots, \mathbf{h}_K$ ($\mathbf{h}_i \in C^{M\times 1}$) are the channel vectors of users $1 \sim K$, the vector $\mathbf{s} \in C^{M\times 1}$ is the transmitted signal, and $n_1, \ldots, n_K$ are independent complex Gaussian noise with variance σ^2. $\mathbf{H} = \left[\mathbf{h}_1 \quad \mathbf{h}_2 \quad \ldots \quad \mathbf{h}_K\right]^H$ is a complex $K \times M$ matrix with the ith row equal to the channel vector of the ith receiver. The transmitted signal has a total power constraint of P, that is $E\left[\|\mathbf{s}\|^2\right] \le P$.

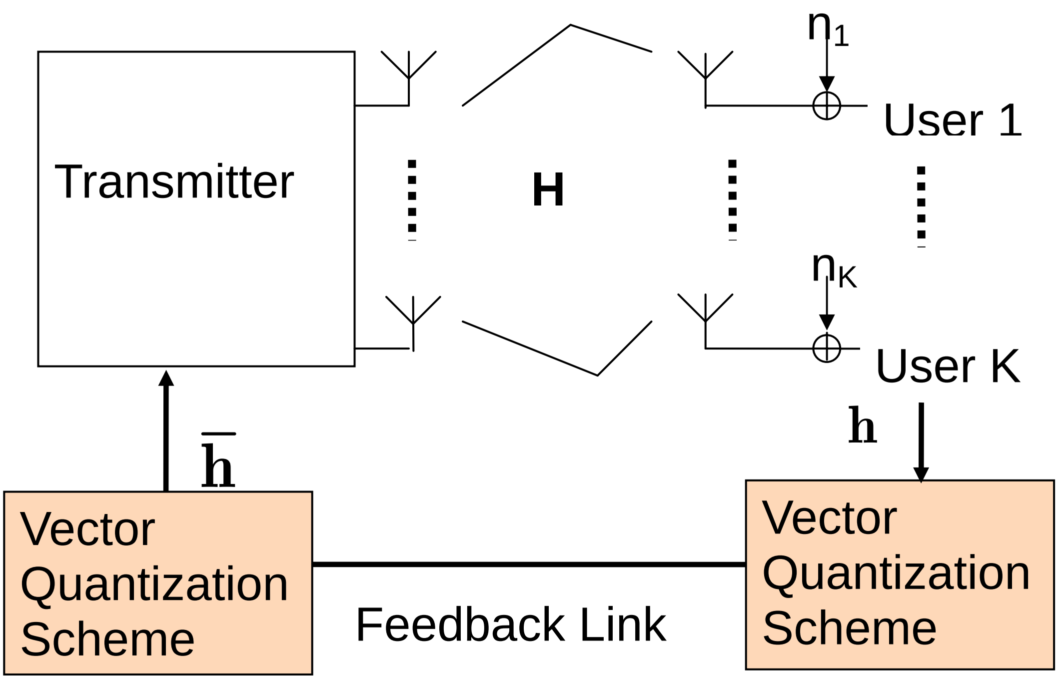

Fig. 2-1 Limited feedback multi-user MIMO system

Each receiver is assumed to have perfect and instantaneous knowledge of its own channel vector, i.e., $\mathbf{h}_i$, and the feedback link is zero-delay. The receiver quantizes its channel by a vector quantization algorithm which is designed to minimize some distortion function like mean squared error (MSE) between the channel vector and quantized vector (i.e., codeword). The codebook with 2^B codewords $C \triangleq \{\mathbf{c}_1 \quad \mathbf{c}_2 \quad \dots \quad \mathbf{c}_{2^B}\}$ is known at both transmitter and receiver. Quantized CSI $\bar{\mathbf{h}}_i$ is fed back from each mobile receiver to the transmitter for further processing.

2.2 Precoding Scheme

The performance of linear precoding depends on the choice of beamforming vectors. One simple choice of beamforming vectors is the zero-forcing vectors, which are chosen such that no multiuser interference is experienced at any of the receivers. Zero-forcing precoding is a low complexity precoding scheme whose performance is asymptotically optimal among the linear precoders at high SNR[19]. If the perfect CSI is known at the transmitter, zero-forcing can be used to completely eliminate multiuser interference. This creates a interfering-free channel to each of the K receivers and thus leads to a multiplexing gain of K. In the finite rate feedback system, the transmitter only knows the partial information about CSI. For example, the beamforming vectors of the zero-forcing precoder are selected based on the quantized channel vectors.

Let $\bar{\mathbf{h}}_i$ denote the quantized channel vector of mobile user i. These quantized vectors are compiled into a matrix $\bar{\mathbf{H}} = \begin{bmatrix} \bar{\mathbf{h}}_1 & \bar{\mathbf{h}}_2 & \cdots & \bar{\mathbf{h}}_K \end{bmatrix}^H$. The unnormalized precoding matrix is $\bar{\mathbf{V}} = \bar{\mathbf{H}}^H (\bar{\mathbf{H}}\bar{\mathbf{H}}^H)^{-1}$. The normalized precoding matrix is $\mathbf{V} = \begin{bmatrix} \mathbf{v}_1 & \mathbf{v}_2 & \cdots & \mathbf{v}_K \end{bmatrix}$, where $\mathbf{v}_i$ is the corresponding unit norm beamforming vector for user i. Also, the transmitted signal is $\mathbf{s} = \sum_{j=1}^{K} \mathbf{v}_j x_j$, x_j is the symbol intended for the i^{th} user. Thus the received signal at user i is

$$y_i = \mathbf{h}_i^H \mathbf{s} + n_i = \mathbf{h}_i^H \sum_{j=1}^{K} \mathbf{v}_j x_j + n_i, \tag{2.2}$$

and the SINR at user i is

$$\mathrm{SINR_i} = \frac{\frac{P}{K} \left| \mathbf{h}_i^H \mathbf{v}_i \right|^2}{\sigma^2 + \frac{P}{K} \sum_{i \neq j} \left| \mathbf{h}_i^H \mathbf{v}_j \right|^2}. \tag{2.3}$$

.

2.3 Correlated Channel Model

The Rayleigh fading process of the mobile radio channel follows WSS uncorrelated scattering model. The mobile user is moving at a speed of v while the transmitter is fixed. The theoretical power spectral density of the received fading signal has the well-known U-shaped form[20]

$$S(f) = \begin{cases} \dfrac{1}{\pi f_d \sqrt{1-\left(\dfrac{f}{f_d}\right)^2}}, & |f| \le f_d \\ 0\,, & \text{elsewhere} \end{cases}, \tag{2.4}$$

where f_d is the maximum Doppler frequency, given by $f_d = \dfrac{v}{\lambda}$, v is the speed of the mobile user and λ is the wave length of the carrier wave. The normalized continuous time autocorrelation of the received fading signal is given by the zeroth-order Bessel function of the first kind[20] $r(\tau) = J_0\left(2\pi f_d \tau\right)$, where τ is the time delay.

In this thesis, Jakes' channel simulator (see Figure 2.2) is used as the temporal correlated channel. One of the reasons of using Jakes' simulator is that the autocorrelation and, hence, the power spectral density of received signal can be very close to those of the theoretical Rayleigh fading WSS US channel (see Figure 2.3). The model generates fading channel as a sum of M sinusoids defined by the following equation:

$$\begin{aligned} h(t) &= \sqrt{2}\{[2\sum_{n=1}^{M}\cos\beta_n \cos 2\pi f_n t + \sqrt{2}\cos\alpha\cos 2\pi f_D t] \\ &\quad + j[2\sum_{n=1}^{M}\sin\beta_n \cos 2\pi f_n t + \sqrt{2}\cos\alpha\cos 2\pi f_D t]\} \\ &= h_I(t) + jh_Q(t)\,, \end{aligned} \tag{2.5}$$

the parameters are defined in[21] .

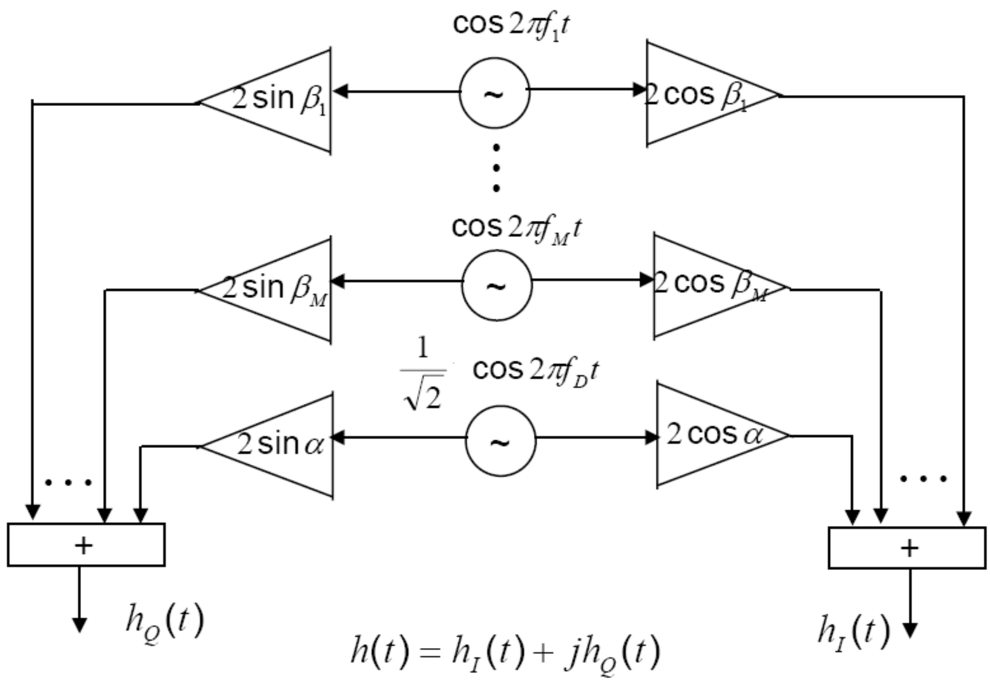

Fig. 2-2 Jakes' fading simulator

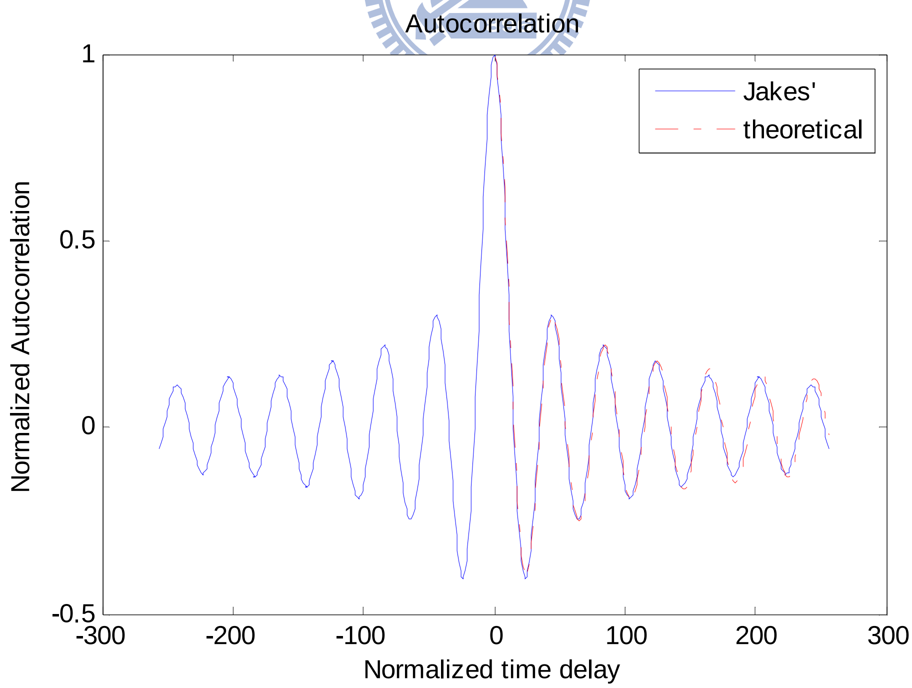

Fig. 2-3 Autocorrelation of Jakes' simulator under $M = 16$

2.4 Quantization Criterion and Codebook Construction in LTE Release 8

Different from conventional vector quantization criterion which often minimizes the mean squared error $\left|\mathbf{h} - \mathbf{c}_l\right|^2$, the quantization criterion in limited feedback systems is aimed to quantize the direction of the channel vector [22-24]. The user chooses the codeword which maximizes the correlation or, equivalently, minimizes the angle between the channel vector and selected codeword, and then feeds back the codeword index to the transmitter (**Fig. 2-4**). The index of selected codeword is

$$q = \arg \max_{l=0,\ldots,2^B-1} \left|\mathbf{h}_i^H \mathbf{c}_l\right|. \tag{2.6}$$

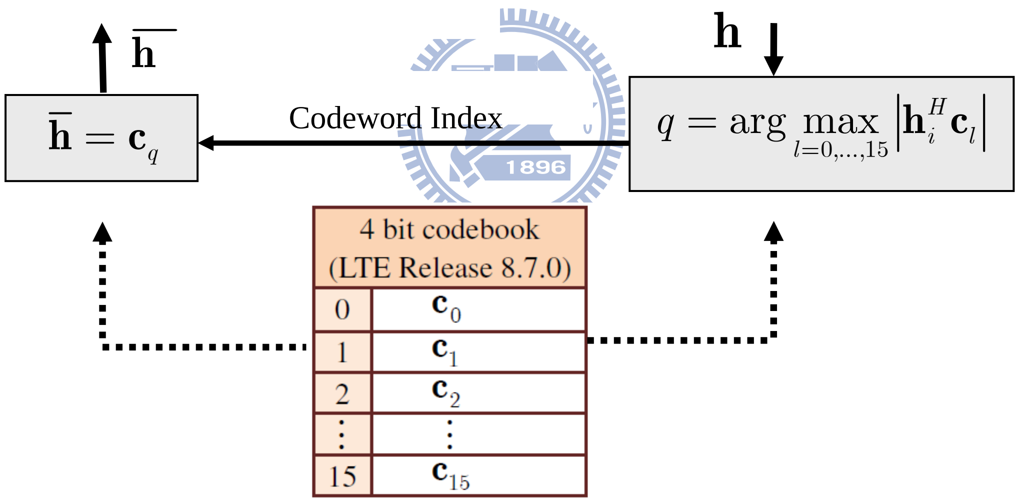

Fig. 2-4 Full vector quantization

Clearly, the codebook generation is always a crucial issue because codebook is a dominant factor for the quality of CSI provided to the transmitter. In this thesis, we introduce LTE 4-bit codebook [25] for our limited feedback system as shown in **Fig. 2-4**. The user selects a codeword from LTE codebook based on the quantization criterion in (2.6). We call this quantization scheme in our limited feedback system "Full Vector Quantization" hereinafter.

Generally, each mobile user uses different codebooks to prevent multiple users from quantizing their channels to the same codeword. The codebook construction in LTE Release 8 is given in **Table 2-1**. There are sixteen generating vectors $\{u_0, u_1, \ldots, u_{15}\}$ and these vectors result in sixteen 4×4 matrices W_n which is defined by

$$W_n = I - \frac{2u_n u_n^H}{u_n^H u_n}, \tag{2.7}$$

where I is the 4×4 identity matrix. In **Table 2-1,** $W_n^{\{p\}}$ denotes the matrix defined by the columns given by the set $\{p\}$. For example, $W_n^{\{13\}}$ is a 4×2 matrix formed from the first and the third columns of W_n.

For single user case (1 layer), $W_n^{\{1\}}$, i.e., the first columns of all W_n $(n = 0, 1, \ldots, 15)$, total sixteen 4×1 vectors, are used as the codebook. For two users (2 layers), $W_n^{\{(1)\}}$ are used as the codebook for the user 1 and $W_n^{\{(2)\}}$ are used for user 2 where $\{(i)\}$ is ith element in the braces. Similarly, for three users (3 layers), $W_n^{\{(1)\}}, W_n^{\{(2)\}}, W_n^{\{(3)\}}$ correspond to the codebooks of users 1-3, and for four users (4 layers), $W_n^{\{(1)\}}, W_n^{\{(2)\}}, W_n^{\{(3)\}}, W_n^{\{(4)\}}$ correspond to the codebooks of users 1-4.

Table 2-1 4-bit Codebook Construction [25]

Codebook index	u_n	Number of layers υ			
		1	2	3	4
0	$u_0 = \begin{bmatrix} 1 & -1 & -1 & -1 \end{bmatrix}^T$	$W_0^{\{1\}}$	$W_0^{\{14\}}/\sqrt{2}$	$W_0^{\{124\}}/\sqrt{3}$	$W_0^{\{1234\}}/2$
1	$u_1 = \begin{bmatrix} 1 & -j & 1 & j \end{bmatrix}^T$	$W_1^{\{1\}}$	$W_1^{\{12\}}/\sqrt{2}$	$W_1^{\{123\}}/\sqrt{3}$	$W_1^{\{1234\}}/2$
2	$u_2 = \begin{bmatrix} 1 & 1 & -1 & 1 \end{bmatrix}^T$	$W_2^{\{1\}}$	$W_2^{\{12\}}/\sqrt{2}$	$W_2^{\{123\}}/\sqrt{3}$	$W_2^{\{3214\}}/2$
3	$u_3 = \begin{bmatrix} 1 & j & 1 & -j \end{bmatrix}^T$	$W_3^{\{1\}}$	$W_3^{\{12\}}/\sqrt{2}$	$W_3^{\{123\}}/\sqrt{3}$	$W_3^{\{3214\}}/2$
4	$u_4 = \begin{bmatrix} 1 & (-1-j)/\sqrt{2} & -j & (1-j)/\sqrt{2} \end{bmatrix}^T$	$W_4^{\{1\}}$	$W_4^{\{14\}}/\sqrt{2}$	$W_4^{\{124\}}/\sqrt{3}$	$W_4^{\{1234\}}/2$
5	$u_5 = \begin{bmatrix} 1 & (1-j)/\sqrt{2} & j & (-1-j)/\sqrt{2} \end{bmatrix}^T$	$W_5^{\{1\}}$	$W_5^{\{14\}}/\sqrt{2}$	$W_5^{\{124\}}/\sqrt{3}$	$W_5^{\{1234\}}/2$
6	$u_6 = \begin{bmatrix} 1 & (1+j)/\sqrt{2} & -j & (-1+j)/\sqrt{2} \end{bmatrix}^T$	$W_6^{\{1\}}$	$W_6^{\{13\}}/\sqrt{2}$	$W_6^{\{134\}}/\sqrt{3}$	$W_6^{\{1324\}}/2$
7	$u_7 = \begin{bmatrix} 1 & (-1+j)/\sqrt{2} & j & (1+j)/\sqrt{2} \end{bmatrix}^T$	$W_7^{\{1\}}$	$W_7^{\{13\}}/\sqrt{2}$	$W_7^{\{134\}}/\sqrt{3}$	$W_7^{\{1324\}}/2$
8	$u_8 = \begin{bmatrix} 1 & -1 & 1 & 1 \end{bmatrix}^T$	$W_8^{\{1\}}$	$W_8^{\{12\}}/\sqrt{2}$	$W_8^{\{124\}}/\sqrt{3}$	$W_8^{\{1234\}}/2$
9	$u_9 = \begin{bmatrix} 1 & -j & -1 & -j \end{bmatrix}^T$	$W_9^{\{1\}}$	$W_9^{\{14\}}/\sqrt{2}$	$W_9^{\{134\}}/\sqrt{3}$	$W_9^{\{1234\}}/2$
10	$u_{10} = \begin{bmatrix} 1 & 1 & 1 & -1 \end{bmatrix}^T$	$W_{10}^{\{1\}}$	$W_{10}^{\{13\}}/\sqrt{2}$	$W_{10}^{\{123\}}/\sqrt{3}$	$W_{10}^{\{1324\}}/2$
11	$u_{11} = \begin{bmatrix} 1 & j & -1 & j \end{bmatrix}^T$	$W_{11}^{\{1\}}$	$W_{11}^{\{13\}}/\sqrt{2}$	$W_{11}^{\{134\}}/\sqrt{3}$	$W_{11}^{\{1324\}}/2$
12	$u_{12} = \begin{bmatrix} 1 & -1 & -1 & 1 \end{bmatrix}^T$	$W_{12}^{\{1\}}$	$W_{12}^{\{12\}}/\sqrt{2}$	$W_{12}^{\{123\}}/\sqrt{3}$	$W_{12}^{\{1234\}}/2$
13	$u_{13} = \begin{bmatrix} 1 & -1 & 1 & -1 \end{bmatrix}^T$	$W_{13}^{\{1\}}$	$W_{13}^{\{13\}}/\sqrt{2}$	$W_{13}^{\{123\}}/\sqrt{3}$	$W_{13}^{\{1324\}}/2$
14	$u_{14} = \begin{bmatrix} 1 & 1 & -1 & -1 \end{bmatrix}^T$	$W_{14}^{\{1\}}$	$W_{14}^{\{13\}}/\sqrt{2}$	$W_{14}^{\{123\}}/\sqrt{3}$	$W_{14}^{\{3214\}}/2$
15	$u_{15} = \begin{bmatrix} 1 & 1 & 1 & 1 \end{bmatrix}^T$	$W_{15}^{\{1\}}$	$W_{15}^{\{12\}}/\sqrt{2}$	$W_{15}^{\{123\}}/\sqrt{3}$	$W_{15}^{\{1234\}}/2$

2.5 Summary

In this chapter, the limited feedback MIMO system is presented. We introduce the 4-bit codebook in LTE Release 8 for full vector quantization in our system. The user feeds back optimum codeword (i.e., quantized CSI) to the transmitter and transmitter performs Zero-Forcing precoding based on these received quantized CSI from different users. Moreover, Jakes' channel simulator is given as our temporal correlated channel model and we will further exploit this temporal correlation of CSI to reduce the number of feedback bits by proposed differential quantization scheme in the next chapter.

Chapter 3

Reduced CSI Feedback Based on Differential Quantization

In limited feedback systems, perfect CSI feedback is impossible due to finite-rate feedback link. How to reduce CSI feedback overhead in limited feedback systems while maintaining performance has became a crucial issue. Differential pulse code modulation (DPCM) gives us the motivation to apply the concept of differential quantization in limited feedback systems to reduce or, equivalently, to compress the number of feedback bits. We further extend DPCM to “Predictive Vector Quantization” (PVQ) [15] to implement differential quantization and thereby reduce the number of feedback bits required. The architecture of PVQ and its components, including a vector quantizer and a predictor, are presented in this chapter.

First, we use differential quantization to feedback CSI by exploiting its temporal correlation. Then, extend to feedback the subcarrier information of MIMO OFDM systems by exploiting the temporal correlation of subcarriers. Simulation results have shown that limited feedback systems with differential quantization scheme can achieve higher SINR under highly correlated channel environment.

3.1 Motivation

Differential quantization is frequently used in data compression or source coding to reduce the number of quantization bits. The most commonly used technique for differential quantization is "differential pulse code modulation" (DPCM) [26]. Intuitively, we can apply DPCM in limited feedback systems to reduce the number of feedback overhead. In **Fig. 3-1**, 1 bit per element, real and imaginary part separately, is assumed (i.e., 8 bits for each channel vector $\mathbf{h} \in C^{4\times1}, M = 4$) for both DPCM and full scalar quantization. **Fig. 3-1** shows higher SINR can be achieved by DPCM compared to the conventional full scalar quantization. However, DPCM is an "element-wise" quantization scheme which requires a large number of bits to quantize a complex channel vector. Therefore, we propose the idea of using differential vector quantization by "Predictive Vector Qautization" (PVQ) in limited feedback systems to further reduce the feedback overhead.

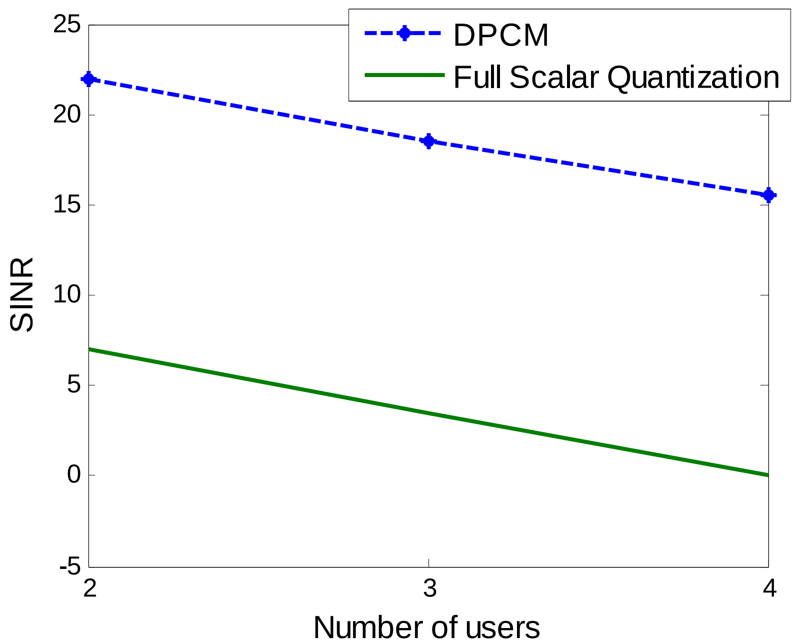

Fig. 3-1 Comparison of DPCM and Full Scalar Quantization

3.2 Proposed Differential Quantization Method

The system model of limited feedback systems with proposed differential VQ scheme is presented in **Fig. 3-2**. We introduce PVQ to implement differential VQ. The block diagrams of PVQ at the transmitter and receiver are shown in **Fig. 3-5** and **Fig. 3-3** respectively. A vector quantizer and a predictor are incorporated at the receiver end while the transmitter end only includes a predictor. The corresponding mathematical expressions of **Fig. 3-3** and **Fig. 3-5** are illustrated in **Fig. 3-4** and **Fig. 3-6** respectively. Instead of quantizing $\mathbf{h}_n$ (full CSI), the difference of channel vector and predicted channel vector, $\mathbf{e}_n = \mathbf{h}_n - \tilde{\mathbf{h}}_\mathbf{n}$ (differential CSI), is quantized. Note that n is denoted as the time index and user index i is ignored here for simplicity. The quantization criterion is

$$\hat{\mathbf{e}}_n = \arg\min_j \left\| \mathbf{e}_n - \mathbf{c}_\mathrm{j} \right\|^2 \tag{3.1}$$

where $\mathbf{c}_\mathrm{j}$, $j = 1, \ldots, 2^{R_d}$ is the codeword from codebook C (R_d is the number of quantization bits for differential CSI). The received quantized $\bar{\mathbf{e}}_\mathbf{n}$ is added by the predicted channel vector $\tilde{\mathbf{h}}_n$ to recover the quantized channel vector $\bar{\mathbf{h}}_\mathbf{n}$

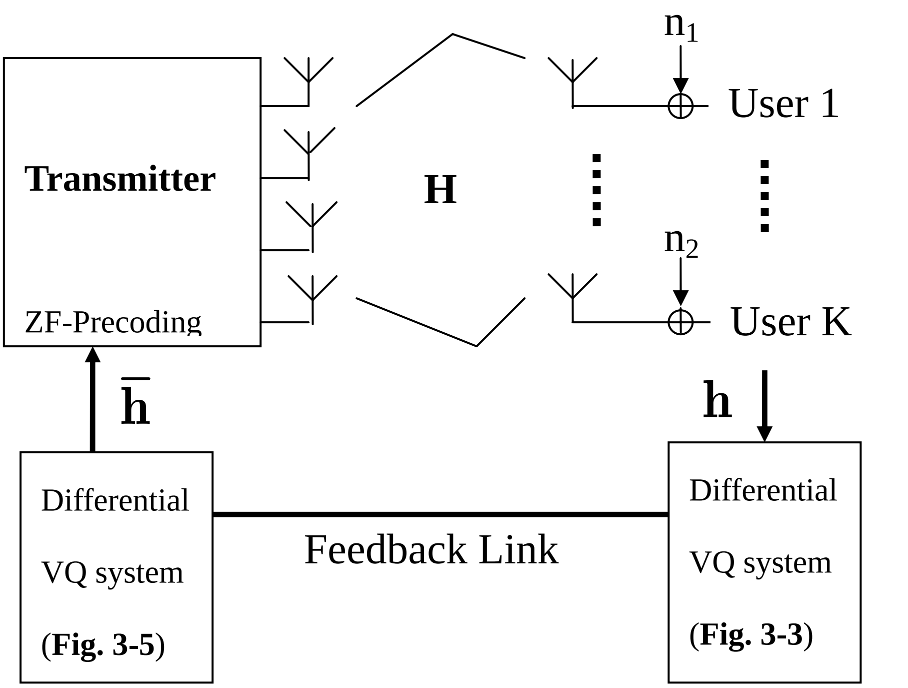

Fig. 3-2 Limited feedback system with proposed differential VQ scheme

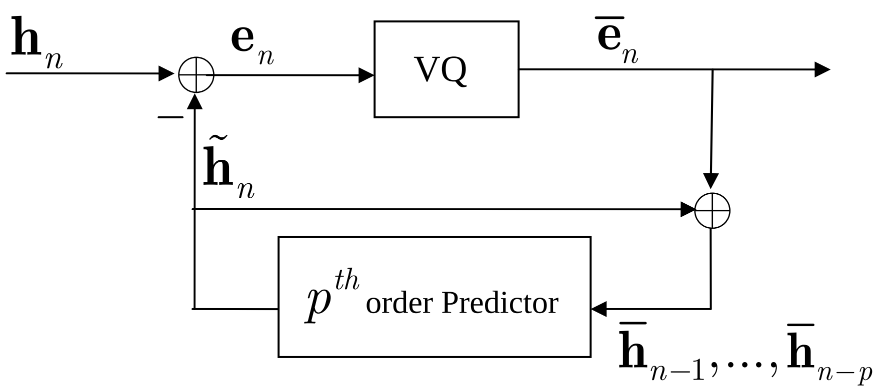

Fig. 3-3 Block diagram of PVQ system at receiver

$$\mathbf{e}_n = \mathbf{h}_n - \tilde{\mathbf{h}}_n$$

$$\bar{\mathbf{h}}_n = \bar{\mathbf{e}}_n + \tilde{\mathbf{h}}_n$$

$$\tilde{\mathbf{h}}_n = -\sum_{k=1}^{p} \mathbf{A}_k \bar{\mathbf{h}}_{n-k}$$

Fig. 3-4 Mathematical expression of PVQ system at receiver

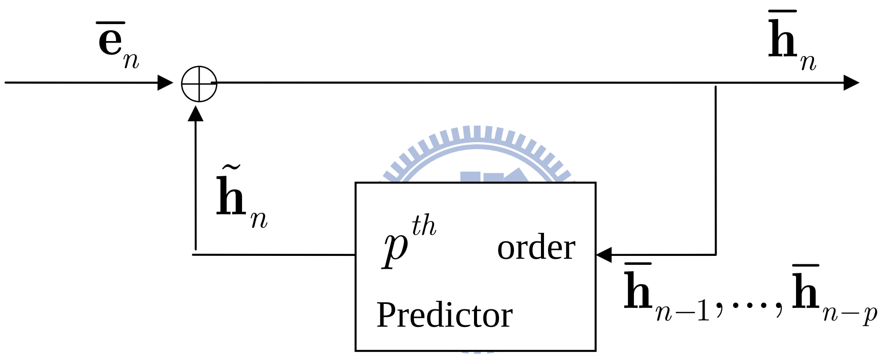

Fig. 3-5 Block diagram of PVQ system at transmitter

$$\tilde{\mathbf{h}}_n = -\sum_{k=1}^{p} \mathbf{A}_k \bar{\mathbf{h}}_{n-k}$$

$$\bar{\mathbf{h}}_n = \bar{\mathbf{e}}_n + \tilde{\mathbf{h}}_n$$

Fig. 3-6 Mathematical expression of PVQ system at transmitter

3.2.1 Incorporation of Predictor

The LMMSE Predictor [27] is incorporated in the proposed differential VQ system. The optimal predictor of LMMSE can be obtained by the "orthogonality principle." Suppose the order of the predictor is p, we can express the orthogonality principle as

$$E\left[\mathbf{e}_n\bar{\mathbf{h}}_{n-i}^H\right] = 0 \qquad \text{for } i = 1,\dots,p, \tag{3.2}$$

that is $E\left[\left(\mathbf{h}_n - \tilde{\mathbf{h}}_n\right)\bar{\mathbf{h}}_{n-i}^H\right] = 0$. Then the channel vector can be predicted as

$$\tilde{\mathbf{h}}_n = -\sum_{k=1}^{p}\mathbf{A}_k\bar{\mathbf{h}}_{n-k}\ , \tag{3.3}$$

where $\mathbf{A}_\mathbf{k} \in C^{M\times M}$. We can rewrite (3.2) as $E\left[\left(\mathbf{h}_n + \sum_{k=1}^{p}\mathbf{A}_k\bar{\mathbf{h}}_{n-k}\right)\bar{\mathbf{h}}_{n-i}^H\right] = 0$, that is

$\mathbf{R}_{0i} = -\sum_{k=1}^{p}\mathbf{A}_k\mathbf{R}_{ki}$ for $i = 1,\dots,p$. Thus $\mathbf{A}_\mathbf{k}$ can be found by the following equation

$$\begin{bmatrix} \mathbf{R}_{11} & \mathbf{R}_{12} & \cdots & \mathbf{R}_{1p} \\ \mathbf{R}_{21} & \mathbf{R}_{22} & & \vdots \\ \vdots & & & \vdots \\ \mathbf{R}_{p1} & \cdots & \cdots & \mathbf{R}_{pp} \end{bmatrix} \begin{bmatrix} \mathbf{A}_1{}^H \\ \mathbf{A}_2{}^H \\ \vdots \\ \mathbf{A}_p{}^H \end{bmatrix} = -\begin{bmatrix} \mathbf{R}_{01} \\ \mathbf{R}_{02} \\ \vdots \\ \mathbf{R}_{0p} \end{bmatrix} \tag{3.4}$$

where $\mathbf{R}_{ij} = E[\mathbf{h}_{n-i}\mathbf{h}_{n-j}^H]$. Since the autocorrelation function of Rayleigh fading WSS US is given by zeroth-order Bessel function of the first kind

$$r(\tau) = J_0\left(2\pi f_d \tau T_s\right),\ \tau = 0,1,2,\dots,.$$

the correlation matrix would simply be $\mathbf{R}_{ij} = E[\mathbf{h}_{n-i}\mathbf{h}_{n-j}^H] = r(|i-j|)\mathbf{I}_M$.

3.2.2 Design of Differential VQ Codebook

For the design of the vector quantization codebook, Generalized Lloyd Algorithm (GLA), which is a widely used codebook generation technique [15, 26], is adopted in our system. The distortion function of GLA is the overall Mean Squared Quantization Error (MSQE) between vectors and quantized vectors.

$$\mathrm{D} = \frac{1}{M}\sum_{m=1}^{M}\left\|\mathbf{x}_m - Q(\mathbf{x}_m)\right\|^2 \tag{3.5}$$

where $\{\mathbf{x}_1, \mathbf{x}_2, \ldots, \mathbf{x}_M\}$ are M sample vectors. GLA training process is shown in **Fig. 3-7**. At the beginning, the initialization of codebook is randomly chosen from the sample vectors. A threshold ε is selected to stop iterations when $D^{(k)} - D^{(k-1)} < \varepsilon$ ($D^{(k)}$ represents the distortion (MSQE) at kth iteration). GLA training process is mainly based on the two rules:

1. Nearest Neighbor Condition: The encoding partition S_n should consist of all vectors that are closer to codeword $\mathbf{c}_n$ than any other codewords.

$$S_n = \left\{\mathbf{x} : \left\|\mathbf{x} - \mathbf{c}_n\right\|^2 \le \left\|\mathbf{x} - \mathbf{c}_{n'}\right\|^2 \ \forall n' \ne n\right\} \tag{3.6}$$

2. Centroid Condition: The codeword $\mathbf{c}_n$ should be average of all the vectors that are in encoding partition S_n.

$$\mathbf{c}_n = \frac{\sum_{\mathbf{x}_m \in S_n} \mathbf{x}_m}{\sum_{\mathbf{x}_m \in S_n} 1} \quad n = 1, 2, \ldots, N \tag{3.7}$$

From **Fig. 3-7**, we learn that GLA requires a large number of sample vectors for training the codebook. If we take a closer look at **Fig. 3-3**, there is one problem: quantized CSI $\bar{\mathbf{h}}_\mathbf{n}$ is required to generate $\mathbf{e}_n$. (i.e., codebook is needed before $\mathbf{e}_n$ generation). The solution for this problem can be solved by two-step codebook training as shown in **Fig. 3-8**.

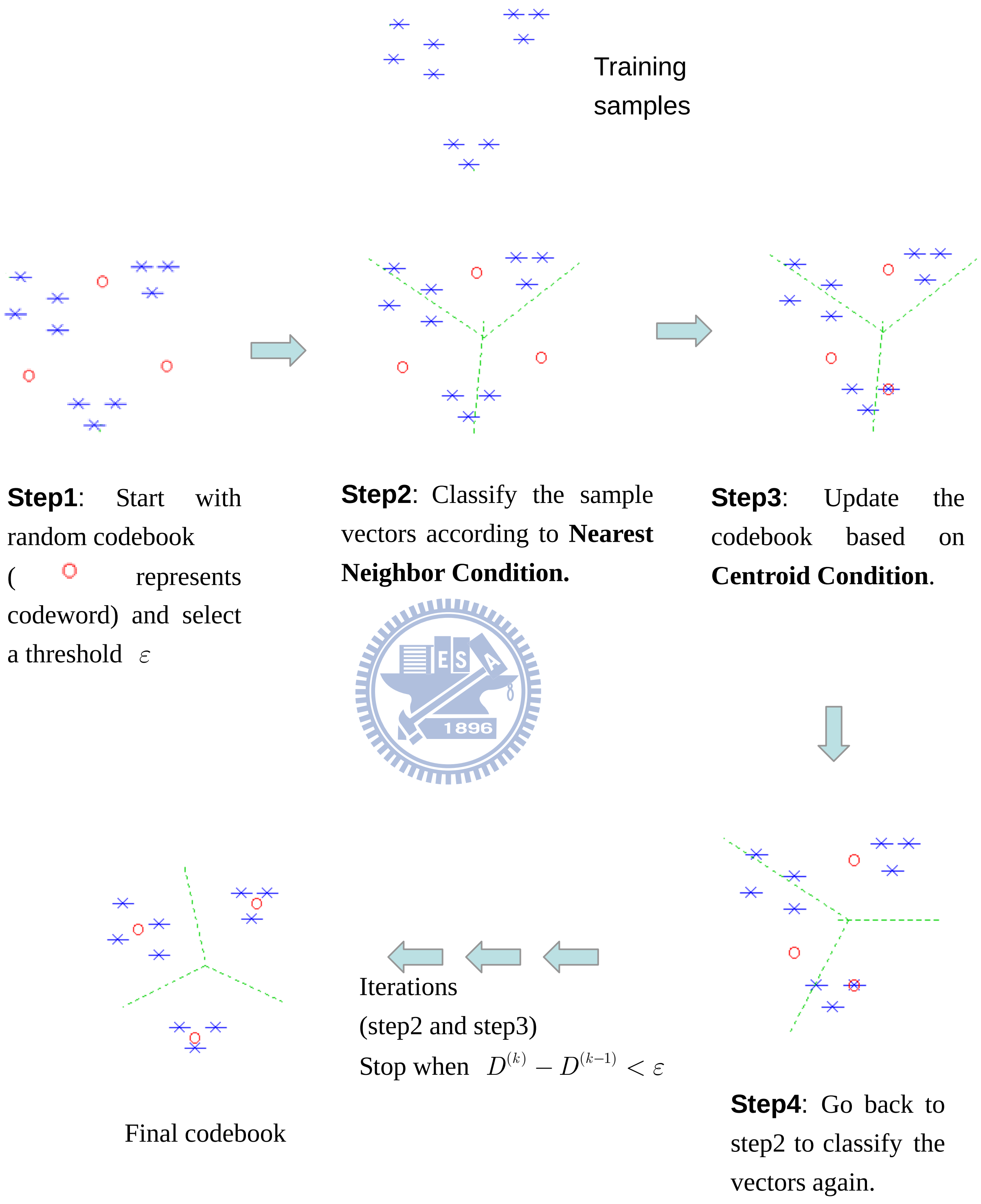

Fig. 3-7 GLA training process [15, 26]

Step 1 is to train the initial codebook by feeding real channel vectors $\mathbf{h}_{\mathbf{n}-1},\ldots,\mathbf{h}_{n-p}$ into the predictor instead of quantized channel vectors $\overline{\mathbf{h}}_{\mathbf{n}-1},\ldots,\overline{\mathbf{h}}_{\mathbf{n}-p}$. Then the initial codebook can be used to generate another bunch of $\mathbf{e}_n$ samples for **Step 2** training. Because the initial codebook is generated by feeding the real channel vectors, the magnitudes of training samples $\mathbf{e}_n$ are smaller than the practical implementation and hence the magnitudes of codewords of initial codebook are also smaller. By **Step 2** training, the codebook would be closer to the practical optimum codebook.

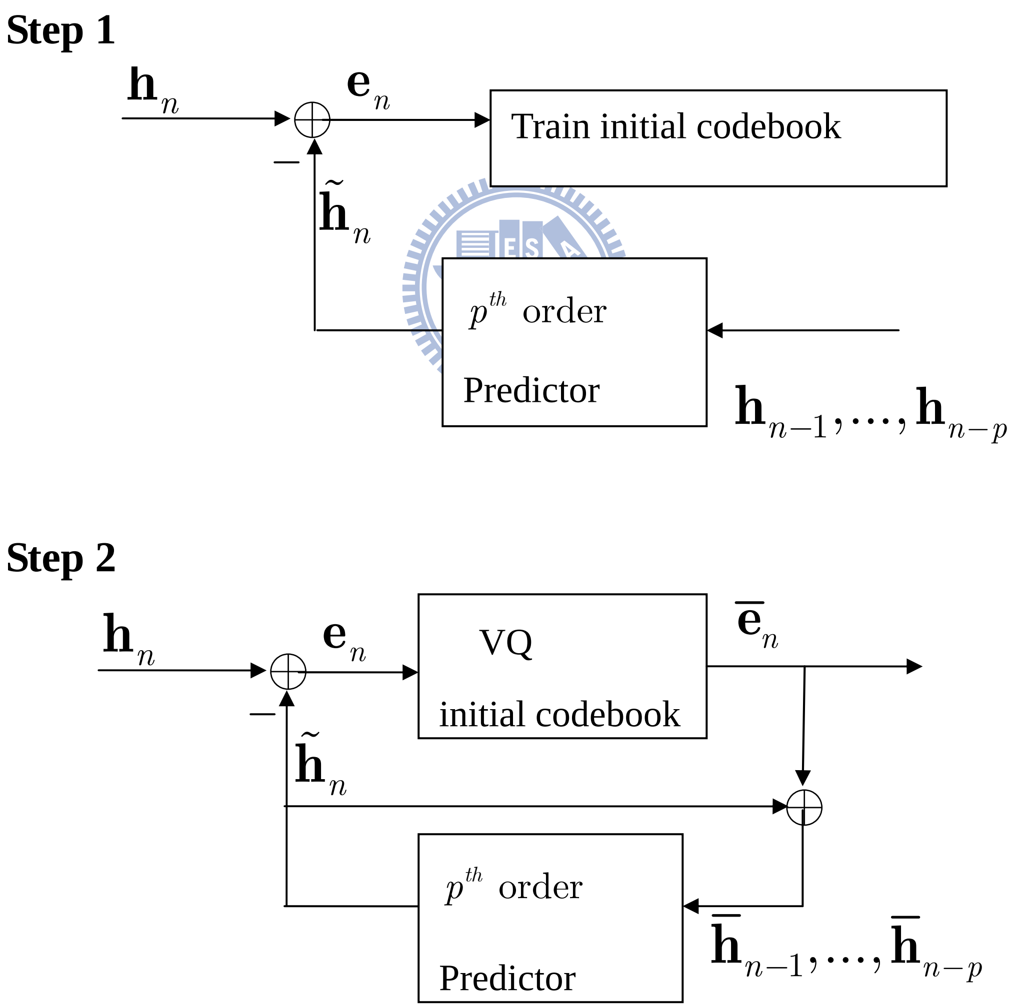

Fig. 3-8 Two-step codebook training

3.2.2 Initial Full CSI and Error Accumulation

Initial Full CSI Quantization

Before differential CSI ($\mathbf{e}_n$) feedback, the first p channel vectors (p is the order of predictor) have to be fed back by full CSI ($\mathbf{h}_n$) quantization. For differential quantization, the accuracy of initial full CSI is a dominant factor of the system performance. Therefore, we quantize initial full CSI "element-wise" by uniform scalar quantization. Separate the real and imaginary parts of each entry in $\mathbf{h} \in C^{M \times 1}$. Then each channel vector $\mathbf{h}$ has $2M$ real elements, and these $2M$ elements are quantized by uniform scalar quantization. Intuitively, the more quantization bits are, the better performance is. **Fig. 3-9** (Two users, the rest of parameter settings are in **Table 3-1**) shows SINR goes up with the number of quantization bits of initial full CSI, R_f, and tends to saturate when R_f is larger than 56 bits (i.e., 7 bits per element).

Error Accumulation Due to Differential Quantization

One major problem for differential quantization is error accumulation. Because the recovered quantized channel vector $\bar{\mathbf{h}}_n$ is based on the past quantized differential CSI vectors ($\bar{\mathbf{e}}_n$), the quantization errors are accumulated over time as shown in **Fig. 3-10** (Two users, the parameter settings are in **Table 3-1** except $R_f = 64 \text{ bits}, R_d = 4 \text{ bits}$). Our solution is to feedback full CSI periodically to maintain CSI quality and correct the past accumulated error. To sum up, we use large number of bits to quantize periodically fed-back full CSIs and few bits to quantize remaining differential CSIs. The average number of feedback overhead is roughly the same as that in Full VQ.

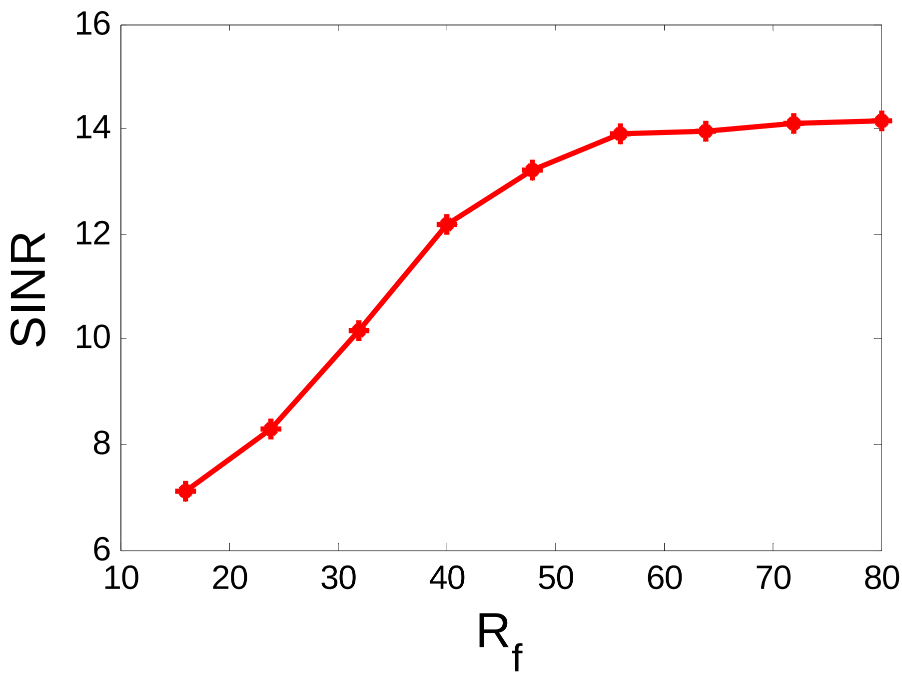

Fig. 3-9 SINR under different number of initial full scalar quantization bits

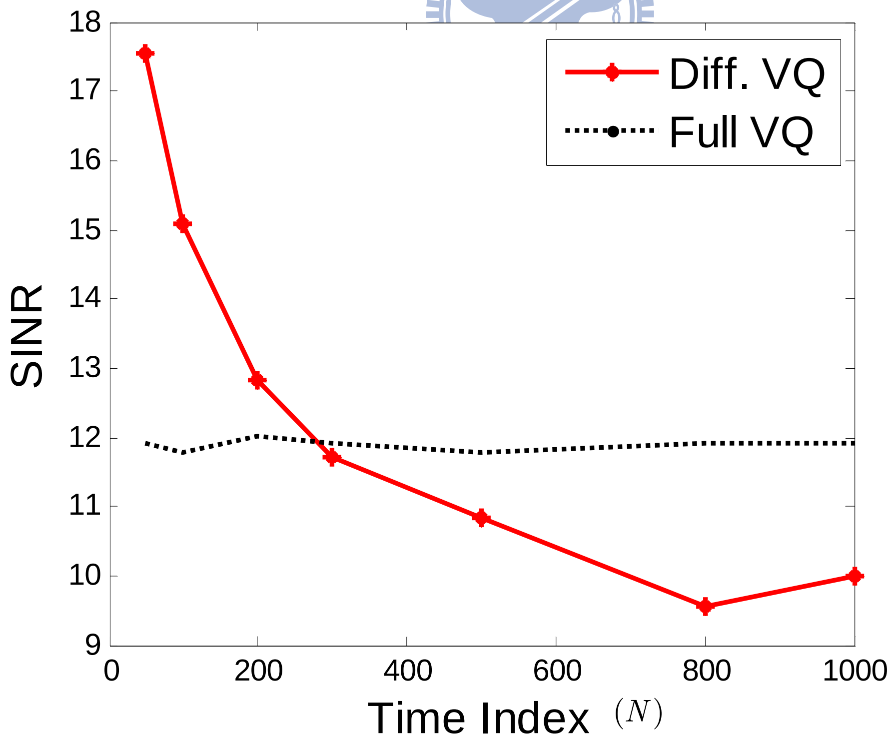

Fig. 3-10 Error Accumulation

3.3 Computer Simulations

In this section, we will give some simulations to demonstrate the advantage of the proposed differential vector quantization scheme. This section is separated into two main simulation environments. The environment in first subsection is the time domain CSI feedback and the environment in second subsection is the frequency domain CSI, i.e., subcarrier information, feedback. Before the demonstration of simulation results, some parameters are defined below.

Definition of Parameters

- Differential CSI feeds back every T_d sec.
- Full CSI feedback every $T_f = N \times T_d$ sec.
- R_f : Number of quantization bits per channel vector for full CSI
- R_d : Number of quantization bits per channel vector for differential CSI
- R_{avg} : Average number of quantization bits per channel vector
- p : Predictor order

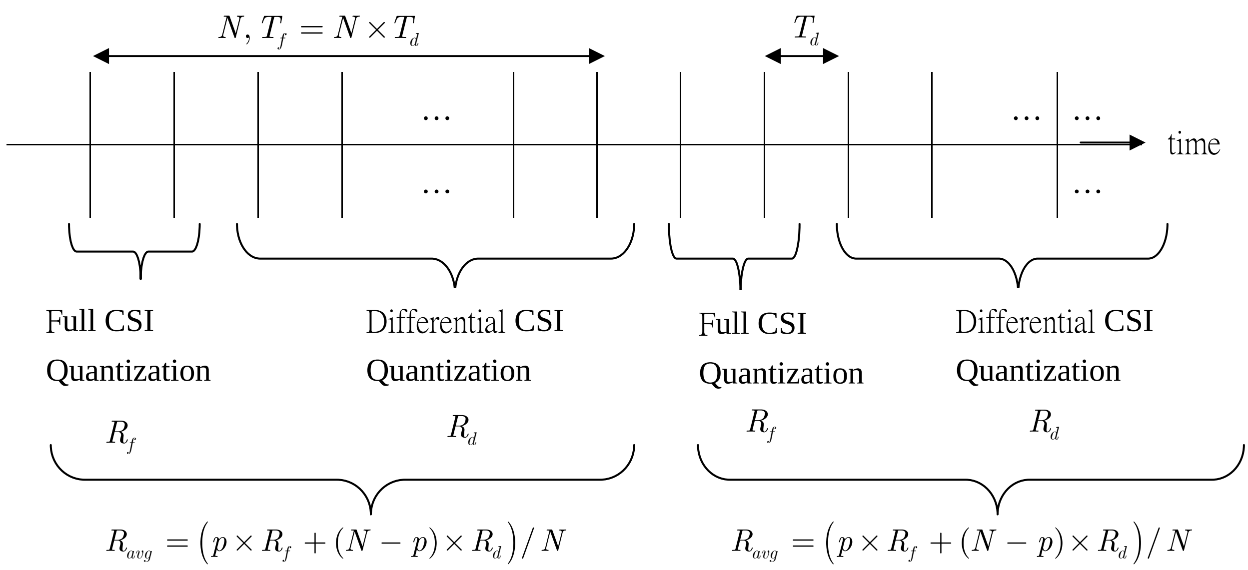

Fig. 3-11 Definition of Parameters

3.3.1 Simulations in Time Domain CSI Feedback

The time domain CSI feedback is considered in this section. **Table 3-1** lists all parameters used in our simulation. The simulation is based on a 4×1 wireless system. Perfect channel knowledge known at the receiver and the error-free feedback channel are also assumed in the simulation. We compare the proposed differential vector quantization to the full vector quantization scheme. The codebook in LTE Release 8 is applied in full VQ. As for the proposed differential VQ, the system uses different self-trained codebooks for different velocities since the users with same velocity should have similar magnitude of codewords. The corresponding codebooks are listed in **Table 3-1**.

Table 3-1 Simulation Parameters

Parameter	Value
Channel	Rayleigh fading channel
Number of Transmit antennas (M)	4
Predictor Order p	2
N	100
T_d	5ms
R_d	3 bits
R_f	56 bits
$R_{avg} = \left(p \times R_f + (N-p) \times R_d\right) / N$	4.06 bits
Carrier frequency f_c	2.5 G Hz
Codebooks (Full VQ)	LTE Release 8 (**Table 2-1**)
Codebooks (Differential VQ)	Self-Trained Codebooks are listed in **Table 3-2** to **Table 3-6**

Table 3-2 codebook for v = 3 km/hr

index	codewords			
1	0.01861- 0.00444i	-0.00301 - 0.00463i	0.00527+ 0.03416i	-0.03592 - 0.01361i
2	-0.00973 - 0.01458i	-0.02546 + 0.05598i	0.00356 - 0.00238i	0.00522 - 0.01194i
3	-0.01701 + 0.05485i	0.01718 + 0.01455i	-0.02505- 0.00429i	-0.00938 - 0.00136i
4	-0.00934- 0.00726i	-0.03289 - 0.02495i	-0.02330- 0.009009i	0.01166 - 0.02058i
5	0.00879 + 0.00057i	-0.00280 - 0.00547i	-0.00072 + 0.00785i	-0.00044 + 0.05364i
6	0.02906 - 0.01368i	0.01717 + 0.00356i	-0.00995 - 0.00238i	0.01279 + 0.00022i
7	-0.00414 + 0.00953i	-0.00462 - 0.01268i	0.04349 - 0.03858i	-0.01125 - 0.00078i
8	-0.03182 - 0.01367i	0.02247 - 0.01104i	0.01172 + 0.01060i	0.01901 - 0.00563i

Table 3-3 codebook for v = 5 km/hr

index	codewords			
1	-0.00254 + 0.01459i	-0.00247 - 0.02514i	0.00051 - 0.01239i	0.034216 - 0.06769i
2	0.01244 + 0.00347i	-0.01007 - 0.02681i	-0.01971 - 0.08106i	-0.003504 + 0.01975i
3	0.00665 + 0.00853i	0.00021 - 0.01303i	0.01479 + 0.00724i	-0.08061 - 0.00688i
4	0.02305 - 0.009834i	-0.00868 - 0.03118i	0.03563 + 0.03017i	0.019476 + 0.01758i
5	-0.00351- 0.00070i	0.00546 - 0.00642i	-0.08181 + 0.04070i	0.00876 + 0.00964i
6	0.01351 + 0.00103i	0.07769 + 0.04163i	0.02180 - 0.00622i	-0.00251 + 0.00760i
7	-0.06896 - 0.03703i	0.00003 + 0.00010i	0.01173 + 0.00265i	0.01042 + 0.01587i
8	0.01214 + 0.01653i	-0.05697 + 0.06416i	0.00512 + 0.00583i	0.00654 + 0.00204i

Table 3-4 codebook for v = 8 km/hr

index	codewords			
1	0.00035 - 0.01122i	0.01596 - 0.001174i	0.00201 + 0.00473i	0.11816 + 0.12526i
2	0.15035 + 0.04310i	-0.00192 - 0.00409i	-0.01544 + 0.01145i	-0.01265 + 0.00132i
3	-0.11170 + 0.11171i	-0.01319 - 0.00398i	0.00558 + 0.01114i	-0.00569 + 0.00489i
4	-0.00363 - 0.02638i	0.02106 - 0.03701i	-0.08108 + 0.11219i	-0.00409 - 0.02105i
5	-0.00838 - 0.02139i	-0.14004 + 0.03852i	-0.01182 - 0.01149i	-0.01468 - 0.01528i
6	-0.01055 - 0.01615i	0.07633 + 0.1015i	-0.04741 - 0.05341i	0.00459 - 0.02524i
7	0.00171 - 0.01931i	0.01484 - 0.03722i	0.08274 - 0.01451i	0.06673 - 0.08474i
8	-0.01458 - 0.04106i	0.020802 - 0.04022i	0.04235 - 0.04929i	-0.10540 + 0.04854i

Table 3-5 codebook for v = 10 km/hr

index	codewords			
1	0.02692- 0.02778i	0.05072 - 0.11008i	0.03964+ 0.09216i	0.07518- 0.10204i
2	-0.20369- 0.08143i	-0.00424- 0.00608i	0.00546+ 0.01879i	-0.01307+0.00941i
3	0.00951+ 0.00001i	-0.01817- 0.02675i	-0.20294- 0.03991i	-0.023612- 0.07295i
4	0.01735- 0.023523i	0.01399- 0.01443i	0.10748- 0.18637i	0.04081- 0.01840i
5	0.03052- 0.02662i	0.14073+ 0.08023i	0.03114+ 0.01050i	-0.10101+ 0.00621i
6	0.02303+ 0.21302i	0.00811+ 0.02800i	0.01418+ 0.00739i	0.01157- 0.01202i
7	0.01571- 0.01906i	0.00910+ 0.01425i	-0.02651+ 0.02517i	0.11569+ 0.18245i
8	0.05089- 0.02973i	-0.16741+ 0.02444i	0.01857+ 0.05147i	-0.05736+ 0.01484i

Table 3-6 codebook for v = 15 km/hr

index	codewords			
1	-0.03156+ 0.01836i	0.23321- 0.27631i	0.00668+ 0.07667i	0.06117+ 0.07148i
2	-0.19797+ 0.29578i	-0.09071+ 0.04809i	-0.05678+ 0.07583i	0.06777- 0.02833i
3	0.05109+ 0.02838i	-0.06168- 0.00099i	0.00341+ 0.03938i	-0.37495+ 0.10158i
4	0.05547 - 0.01414i	-0.10691- 0.03118i	-0.21091- 0.28494i	0.08396+ 0.05085i
5	-0.18560- 0.32995i	-0.08078 - 0.03426i	-0.01932+ 0.04005i	-0.00943- 0.1251i
6	0.27523- 0.02563i	-0.04658+ 0.01468i	-0.04051+ 0.18578i	0.08386- 0.11775i
7	-0.01383- 0.03967i	0.23025+ 0.34098i	-0.03386- 0.05087i	0.04909+ 0.01794i
8	0.02344+ 0.03002i	-0.04260+ 0.004195i	0.36572- 0.11770i	0.03537+ 0.02099i

From the above tables, we can observe that the magnitude of the codewords is larger in the higher speed codebook since for high speed users, the magnitude difference between two consecutive CSI is larger.

Following are three simulation results. The first simulation result in

Fig. 3-12 shows the proposed differential VQ successfully exploits the temporal correlation of channel vectors and can achieve higher SINR compared to full VQ under 5 km/hr environment. If we extend the time of full CSI feedback, average number of bits decrease but SINR degrades. **Fig. 3-14** shows the SINR for different velocities. Because higher velocity results in smaller temporal correlation, smaller correlation of CSI degrades the performance of differential quantization. Unlike differential VQ which suffers from error accumulation, full VQ quantizes channel vector at every time instant independently, so the performance of full VQ is unvarying under different velocities.

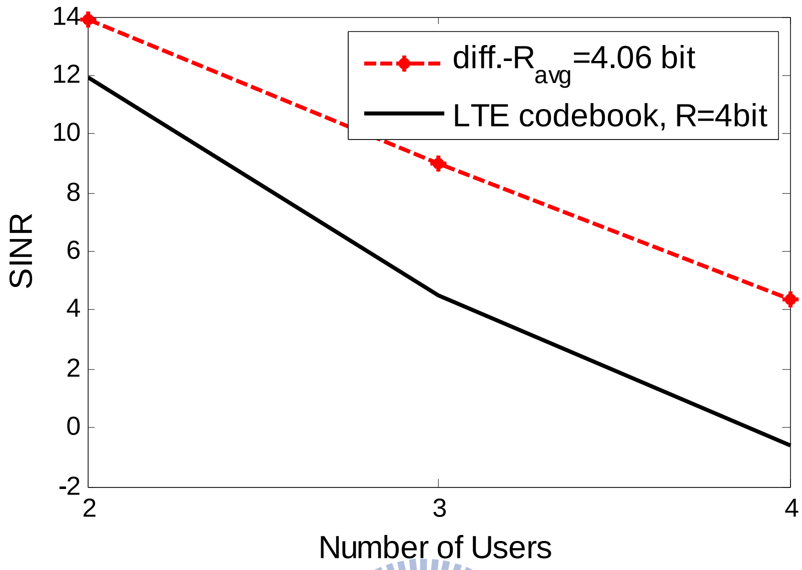

Fig. 3-12 Differential vector quantization vs. Full vector quantization

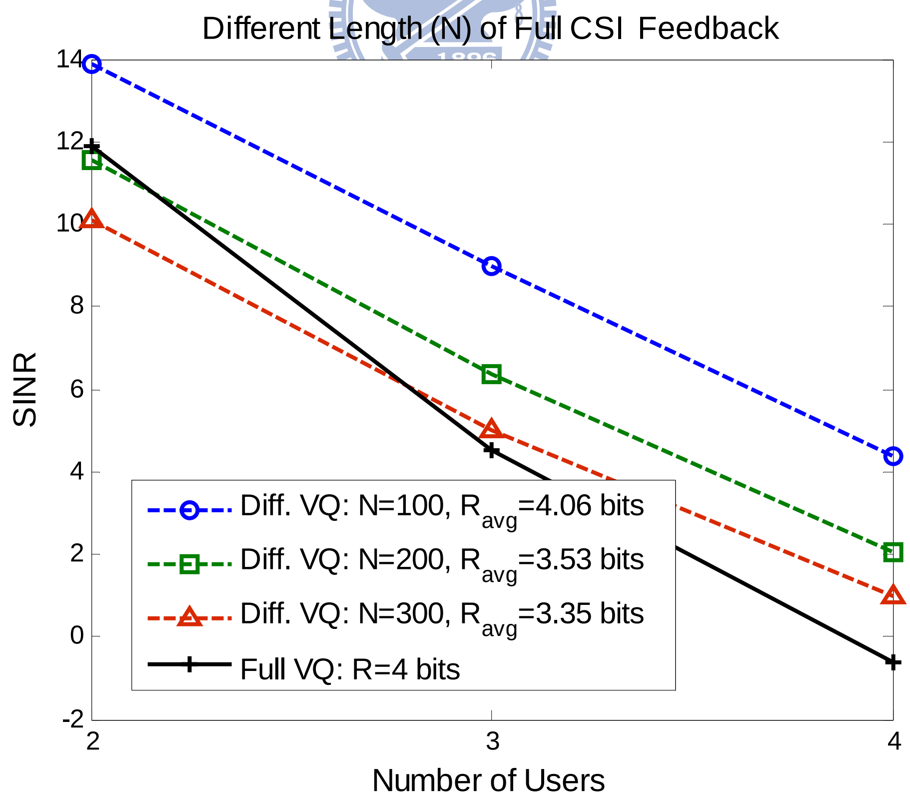

Fig. 3-13 Differential vector quantization under different N (T_f)

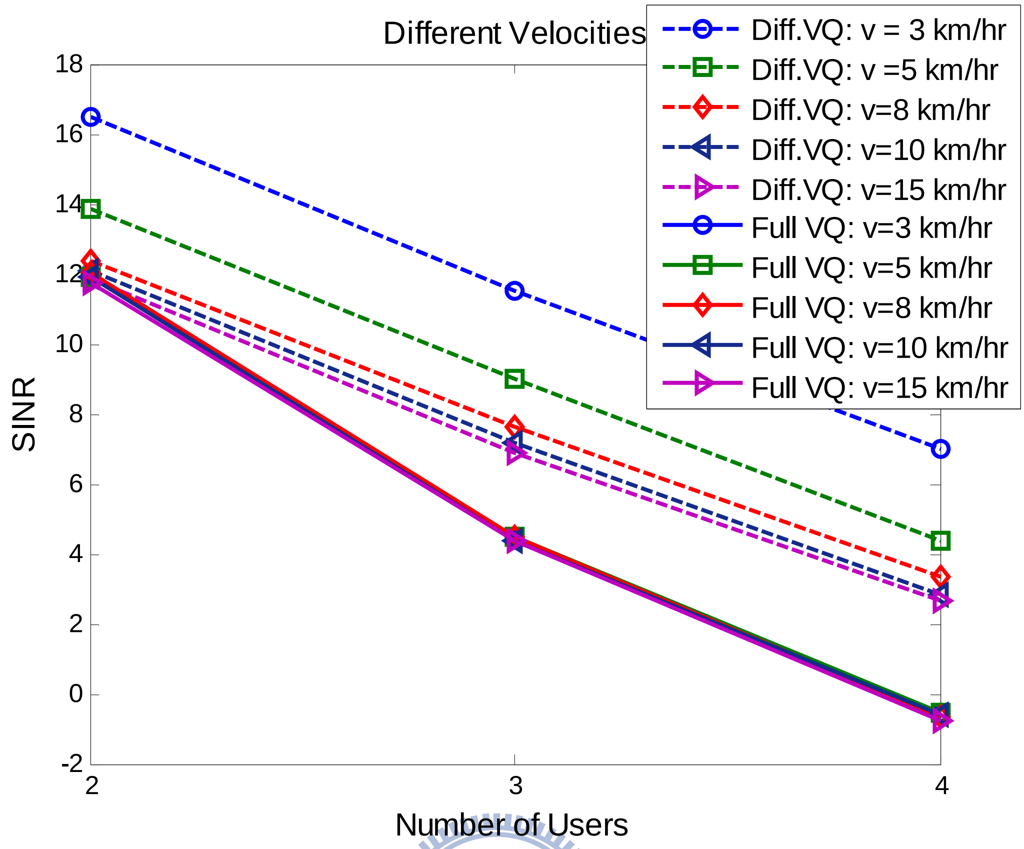

Fig. 3-14 Differential vector quantization under different velocities

3.3.2 Extension to MIMO OFDM system

In LTE frame structure, one radio frame is 10 ms long and consists of 20 slots of length 5 ms. A subframe is defined as two consecutive slots, that is one radio frame is composed of 10 subframes. A physical resource block is defined as N_{symb} $(=7)$ consecutive OFDM/SC-FDMA symbols in the time domain and N_{sc}^{RB} $(=12)$ consecutive subcarriers in the frequency domain. The smallest resource unit is denoted a resource element. Since there are many subcarriers (may up to 1024) in a time instant, it is impossible to feedback all the subcarriers information to the transmitter. Usually, k consecutive resource blocks share one codeword and k depends on different modes in LTE [25]. So only the subcarrier in the mid of k consecutive resource blocks is fed back.

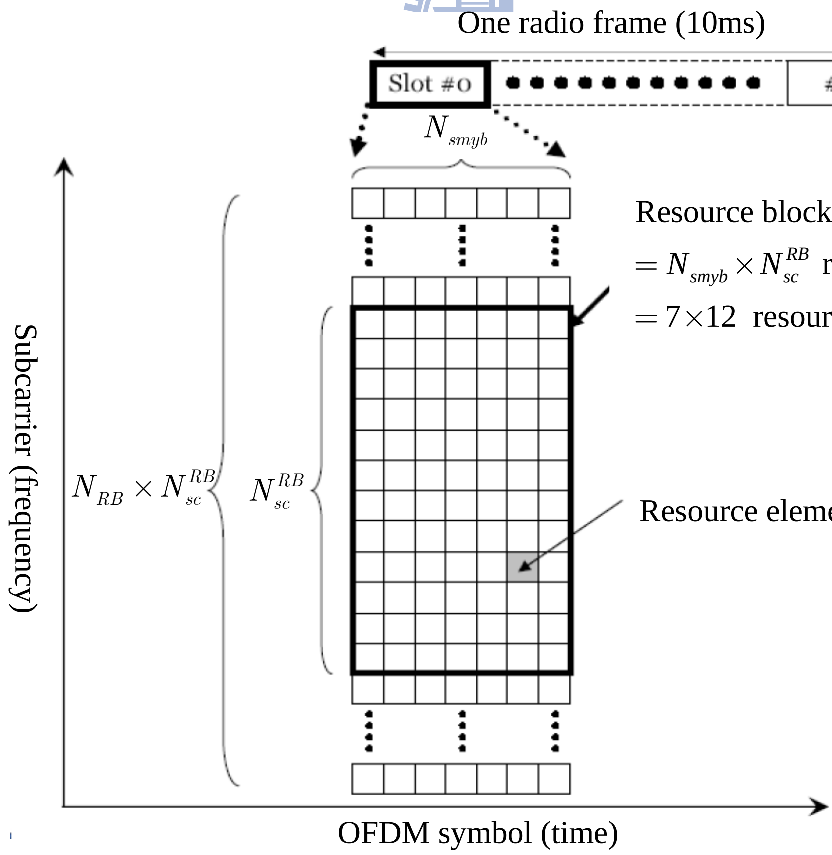

Fig. 3-15 LTE resource grid

Table 3-7 Simulation Parameters

Parameter	Value
Channel	Rayleigh fading channel
Number of transmit antennas (M)	4
Number of users	2-4
Predictor Order p	2
N	100
T_d	5ms
$T_f = N \times T_d$	500ms
R_d	3 bits
R_f	56 bits
$R_{avg} = \left(p \times R_f + (N-p) \times R_d\right) / N$	4.06 bits
k	4
Number of subcarriers	512
Number of multipath **with delays**	6 $[0\ 2\ 4\ 6\ 8\ 10] \times T_d$
Carrier frequency f_c	2.5 G Hz
Codebooks (Full VQ)	LTE Release 8 (**Table 2-1**)
Codebooks (Differential VQ)	Self-Trained Codebooks are listed in 3 km/hr: **Table 3-8** 5 km/hr: **Table 3-9** 8 km/hr: **Table 3-10** 10 km/hr: **Table 3-11** 15 km/hr: **Table 3-12**

Table 3-8 codebook for v = 3 km/hr

index	codewords			
1	0.01850+ 0.01663i	0.15751+ 0.10612i	-0.075845+ 0.09921i	0.12522- 0.18442i
2	0.40755 - 0.26827i	0.18229+ 0.02534i	0.07001+ 0.21347i	0.08667+ 0.07725i
3	0.10392+ 0.24114i	0.09846+ 0.10685i	-0.11746+ 0.06245i	-0.10948+ 0.12052i
4	0.03421+ 0.0204i	-0.15147+ 0.14220i	-0.06990- 0.09554i	0.15874+ 0.22629i
5	-2.00152- 1.08612i	2.39253+ 0.61204i	-1.92461- 1.81288i	0.58650- 0.87042i
6	0.00092- 0.11588i	0.03269 - 0.18963i	0.15093+ 0.01060i	-0.07942- 0.11052i
7	-2.81571- 0.071022i	0.79602- 0.96609i	1.46382- 0.36982i	0.92291+ 1.14374i
8	-0.19272+ 0.13480i	-0.04540+ 0.07487i	-0.08165- 0.09375i	-0.11690- 0.13523i

Table 3-9 codebook for v = 5 km/hr

index	codewords			
1	0.30445+ 0.22635i	0.15751+ 0.10612i	-0.07584+ 0.09921i	0.12522 - 0.18442i
2	0.40755- 0.26827i	0.18229+ 0.02534i	0.07001+ 0.21347i	0.08667 + 0.07725i
3	0.10392+ 0.24114i	0.09846+ 0.10685i	-0.11746+ 0.06245i	-0.10948+ 0.12052i
4	0.03421+ 0.02045i	-0.15147+ 0.14220i	-0.06990- 0.09554i	0.15874+ 0.22629i
5	-2.00152 - 1.08612i	2.39253+ 0.61204i	-1.92416 - 1.81288i	0.58650- 0.87042i
6	0.00092- 0.11588i	0.03269- 0.18963i	0.15093 + 0.01060i	-0.07942 - 0.110529i
7	-2.81571 - 0.07102i	0.79602 - 0.96609i	1.46382 - 0.36988i	0.92291+ 1.14374i
8	-0.19272+ 0.13480i	-0.04540+ 0.07487i	-0.08165- 0.09375i	-0.11690- 0.13523i

Table 3-10 codebook for v = 8 km/hr

index	codewords			
1	-0.30445+ 0.22635i	-0.08192 + 0.30640i	-0.13432+ 0.199751i	0.41735 - 0.14419i
2	-0.15031+ 0.01269i	0.35441+ 0.11945i	0.04724+ 0.20804i	0.08446+ 0.14228i
3	-0.28148- 0.06025i	-0.17323 - 0.00949i	0.17891- 0.19109i	-0.08100- 0.23096i
4	0.10639+ 0.01218i	0.04763+ 0.06343i	-0.0409 - 0.43678i	0.24865+ 0.29275i
5	0.017640- 0.07233i	-0.22372+ 0.28215i	0.063256+ 0.00006i	-0.22293+ 0.24969i
6	0.04519+ 0.19604i	-0.00388- 0.10754i	-0.06925+ 0.27971i	-0.35732- 0.13852i
7	0.29571- 0.15511i	-0.26035- 0.35558i	0.06717- 0.01712i	-0.17588+ 0.02205i
8	0.03268+ 0.06397i	0.31217- 0.31186i	-0.23381- 0.12263i	0.17470- 0.45801i

Table 3-11 codebook for v = 10 km/hr

index	codewords			
1	0.38819- 0.05640i	0.279081- 0.084417i	-0.085771- 0.228474i	0.294287+ 0.50050i
2	-0.26705+ 0.09830i	-0.10912+ 0.27842i	-0.18124- 0.39648i	-0.15851 + 0.34360i
3	0.27077+ 0.36627i	0.00919+ 0.09340i	0.27123+ 0.19372i	-0.37589+ 0.29274i
4	0.033498 - 0.28856i	-0.23501- 0.04900i	0.56626- 0.32576i	-0.06516- 0.04615i
5	0.12185+ 0.30981i	0.02615+ 0.04254i	-0.02207+ 0.25378i	0.43702- 0.31196i
6	-0.35221+ 0.03415i	0.22407- 0.03079i	-0.00789+ 0.168390i	-0.35287- 0.31445i
7	-0.06664 - 0.39172i	-0.21855- 0.15347i	-0.02613+ 0.39965i	0.00177- 0.04736i
8	-0.18204 - 0.47617i	0.13907- 0.05957i	-0.29671- 0.264254i	0.34720- 0.24472i

Table 3-12 codebook for v = 15 km/hr

index	codewords			
1	0.31149- 0.51042i	-0.84816- 0.35939i	0.00875- 0.03616i	-0.55162- 0.09785i
2	0.14076+ 0.32218i	-0.01956+ 0.94223i	0.29629+ 0.24979i	0.116174- 0.74335i
3	-0.11393+ 0.72280i	-0.11386- 0.20279i	-0.41209+ 0.70975i	-0.06094+ 0.49142i
4	-0.62541- 0.14539i	0.50913- 0.50412i	-0.37464 - 0.15517i	-0.03885- 1.05382i
5	0.81650+ 0.38587i	0.38412+ 0.43180i	-0.25944 - 0.55869i	-0.15011+ 0.17496i
6	0.15015- 0.75979i	0.83052+ 0.15415i	0.12825+ 0.12149i	0.43432+ 0.31504i
7	-0.27572+ 0.48021i	0.31749- 0.67221i	0.68262 - 0.49347i	0.36509+ 0.07361i
8	-1.07468- 0.17525i	-0.35833+ 0.58647i	0.20414- 0.10759i	-0.38812+ 0.22483i

Similarly, the codebook for higher velocity users has the larger magnitude of codeword since the temporal correlation of channel is weaker. In MIMO OFDM systems, the temporal correlation is not obvious so the performance tends to degrade compare to that in MIMO systems. But our proposed differential quantization scheme can still attain higher SINR under highly correlated channel environments as shown in **Fig. 3-16**, **Fig. 3-17** and **Fig. 3-18**. Intuitively, the reason for differential VQ is superior to full VQ is that the magnitude of codewords in differential VQ is smaller than those in full VQ. The same size of codebook can represent the differential CSI more precisely compared to full CSI. Therefore, the quantization error will be smaller in our proposed differential VQ scheme.

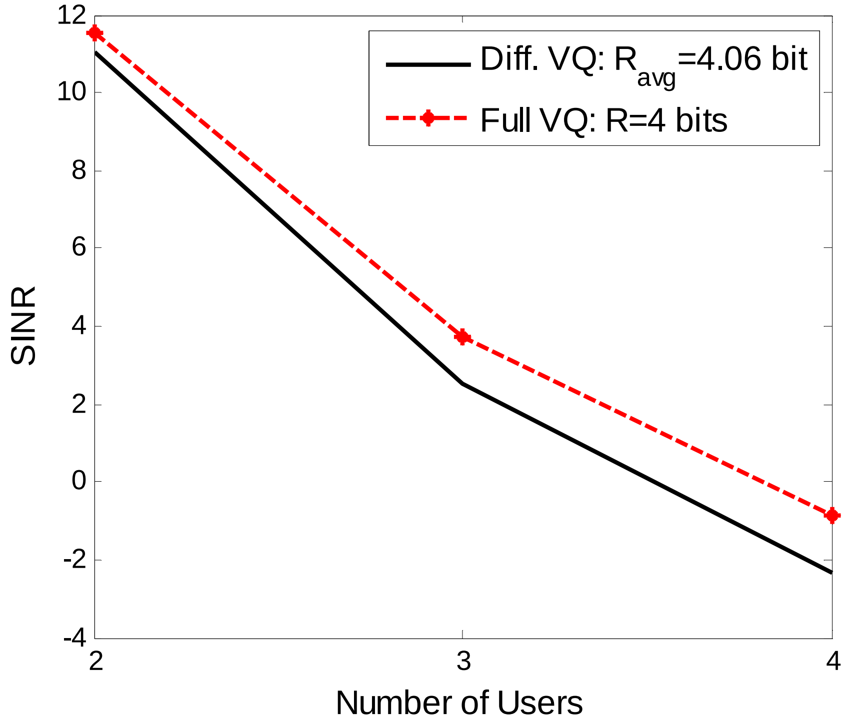

Fig. 3-16 Differential vector quantization vs. Full vector quantization

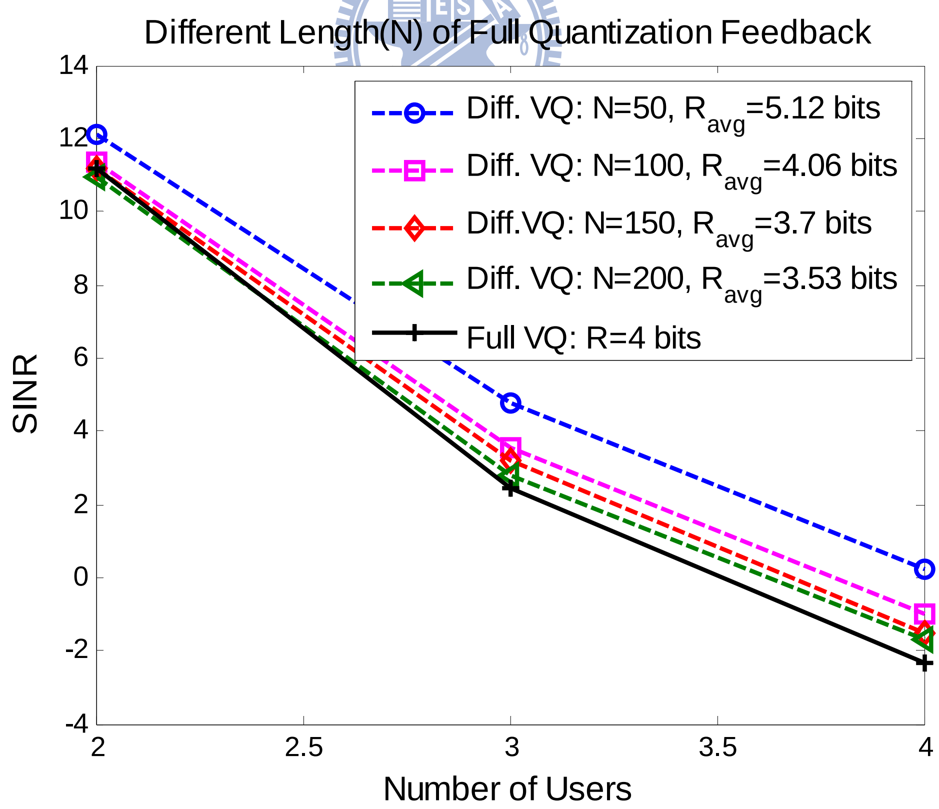

Fig. 3-17 Differential vector quantization under different N (T_f)

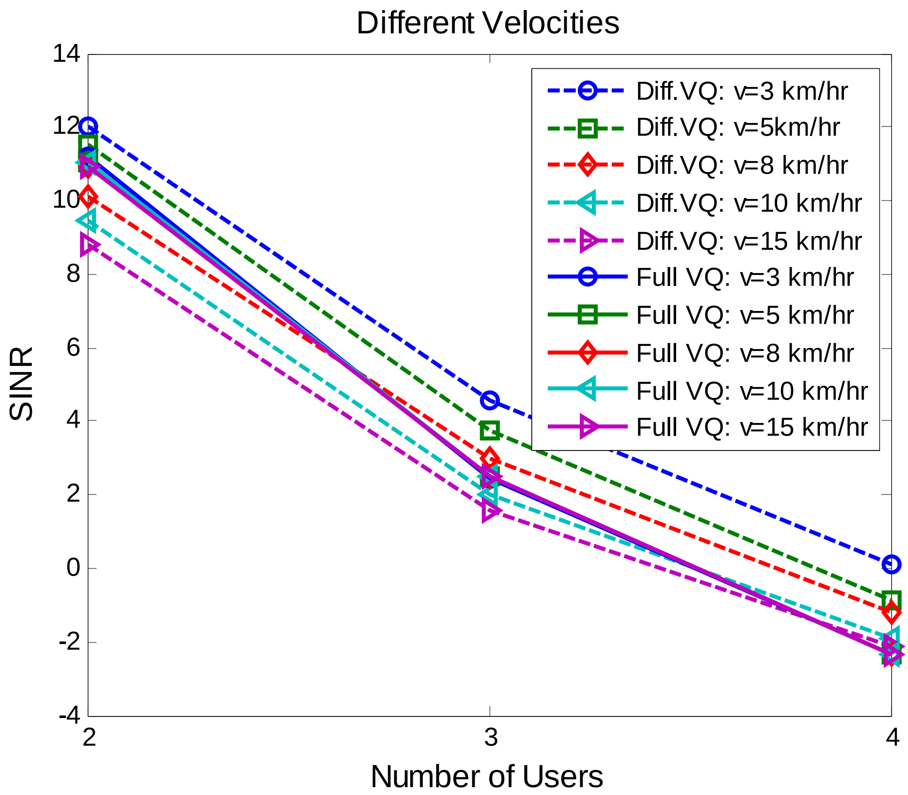

Fig. 3-18 Differential vector quantization under different velocities

3.4 Summary

In this chapter, we apply the concept of differential quantization in data compression to limited feedback systems. The proposed differential vector quantization scheme is presented. We first incorporate the model of PVQ in the limited feedback system. Also, LMMSE predictor is used in our PVQ model. The codebook is trained by GLA with some modifications. The full CSI are periodically fed back in between differential CSI to correct the accumulated error. For full CSI, a large number of quantization bits are used while fewer quantization bits are used for differential CSI. The average feedback overhead is roughly the same as in full VQ. To sum up, the proposed differential vector quantization scheme can attain higher SINR at the expense of a slight increase in feedback overhead compared to full VQ.

Chapter 4

Discussion of Different Feedback Overheads and Spatial Correlation Matrix Feedback

In this chapter, two main topics are addressed; one is discussion of users' performances under different feedback overheads and the other is feedback reduction for spatial correlation matrix via vector quantization. In the previous chapter, all users are permitted to feedback CSI under the same overhead but in the practical communication system, some users might be allowed to have higher feedback overhead. Therefore, the first part of this chapter is mainly to discuss the system performance in different feedback overhead scenarios.

Also, in Chapter 3, the proposed differential vector quantization has been shown to be an effective way to quantize CSI. So, the second part of this chapter aims to further find an effective method to quantize the spatial correlation matrix to reduce the number of quantization bits. Here, we propose diagonal-wise full vector quantization by exploiting the channel spatial correlation. The proposed scheme can achieve a smaller MSE compared to existing methods such as entry-wise differential scalar quantization.

4.1 Different Feedback Overheads in Multi-user Systems

In LTE systems, there are different reporting modes for CSI feedback. Some reporting modes are triggered by scheduling grants and allow mobile users to feedback CSI with higher overhead,. In this section, we are going to discuss about the influence on all mobile users under the scenario in which only some specific users are permitted to have higher feedback overhead. First, a simulation result demonstrates the performance for users with different feedback overheads. Then, discussion of the result will be given under a geometrical point of view.

4.1.1 Simulation Demonstration

In the simulation, we have two simple cases as shown in **Table 4-1**. Only the first user in Case 1 has higher feedback overhead. Other users in Case 1 have the same feedback overhead as the users in Case 2. The simulation parameters are defined in **Table 4-2**. As we can see from **Fig. 4-1**, only first user in Case 1 benefits from the higher cost of feedback overhead. Other users in Case 1 have the same SINR as those users in Case 2. This implies that user performance does not change if some other users in the system are allowed to feedback CSI with higher overheads.

Table 4-1 Two cases in simulation

Case 1	First user: 4 bits/ 12 subcarriers Other users: 4 bits/ 48 subcarriers
Case 2	All the users: 4 bits/ 48 subcarriers

Table 4-2 Simulation Parameters

Parameters	**Value**					
Quantization Scheme	Full vector quantization					
Channel	Multipath Rayleigh fading channel					
Tap	1	2	3	4	5	6
Relative delays (ms)	0	10	20	30	40	50
Number of transmit antennas	4					
Carrier frequency	2.5G Hz					
Velocity	5 km/hr					
Sampling time	5 ms					
Number of subcarriers	512					

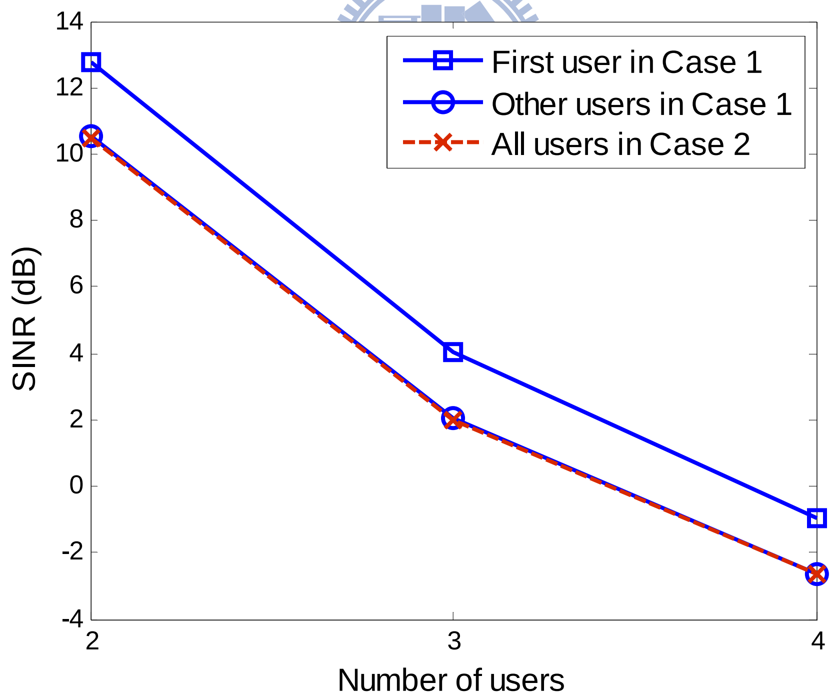

Fig. 4-1 Simulation demonstration of different feedback overheads for different users

4.1.2 Geometric Interpretations

In the following sections, we will analyze the simulation result in **Fig. 4-1** under a geometrical point of view. The geometric representation for a two-user case is shown in **Fig. 4-2**, and the corresponding definitions of parameters are listed in **Table 4-3**.

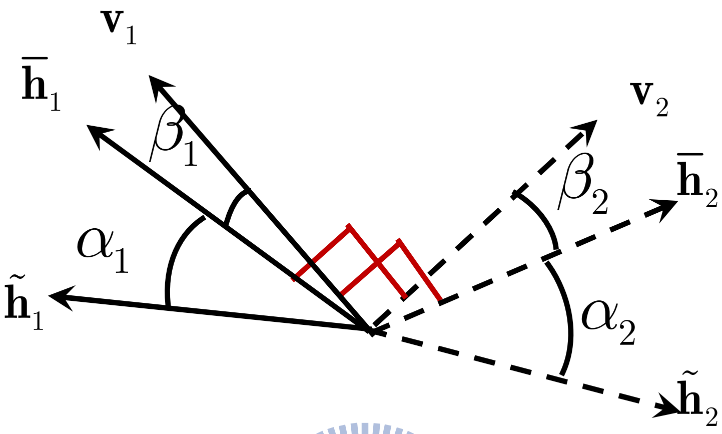

Fig. 4-2 Geometric representation for two users case

Table 4-3 Definitions of parameters

Parameters	Definitions
$\tilde{\mathbf{h}}_i$	Normalized channel vector for user i
$\bar{\mathbf{h}}_i$	Quantized channel vector for user i
$\mathbf{v}_i$	Beamforming vector for user i
α_i	Quantization angular error between $\tilde{\mathbf{h}}_i$ and $\bar{\mathbf{h}}_i$
β_i	Angle between $\bar{\mathbf{h}}_i$ and $\mathbf{v}_i$

Since the transmitter performs zero-forcing precoding, the beamforming vector $\mathbf{v}_j$ is orthogonal to the quantized channel vector $\bar{\mathbf{h}}_i$ for $i \neq j$ (i.e., $\bar{\mathbf{h}}_i \perp \mathbf{v}_j, i \neq j$). Also, we have two assumptions here,

1. $\alpha_i < \frac{\pi}{2}$.

   If $\frac{\pi}{2} < \alpha_i < \pi$, the magnitude of $\left|\tilde{\mathbf{h}}_i \bar{\mathbf{h}}_i\right|^2 = \cos^2 \alpha_i$ is equal to $\cos^2(\pi - \alpha_i)$ where $\pi - \alpha_i < \frac{\pi}{2}$. We can always find the equivalent angle which is smaller than $\frac{\pi}{2}$.

2. β_i is small.

   If $\bar{\mathbf{h}}_i$ and $\bar{\mathbf{h}}_j$ $(i \neq j)$ are closely aligned, β_i would be large (close to $\frac{\pi}{2}$) because $\bar{\mathbf{h}}_i \perp \mathbf{v}_j$ which implies $\bar{\mathbf{h}}_j$ and $\mathbf{v}_j$ are nearly orthogonal. And if $\bar{\mathbf{h}}_i$ and $\bar{\mathbf{h}}_j$ $(i \neq j)$ are closely aligned, the problem of singularity, or rank deficiency would happen when the system performs pseudo-inverse in zero-forcing precoding. If we exclude the singular case and $\bar{\mathbf{h}}_i$ and $\bar{\mathbf{h}}_j$ $(i \neq j)$ are nearly orthogonal, we can reasonably assume that β_i is small.

In the following sections, the interferences $\left|\tilde{\mathbf{h}}_i^H \mathbf{v}_j\right|^2$ and precoding gain $\left|\tilde{\mathbf{h}}_i^H \mathbf{v}_i\right|^2$ in SINR of user i

$$\mathrm{SINR}_i = \frac{\frac{P}{K}\left|\mathbf{h}_i^H \mathbf{v}_i\right|^2}{\sigma^2 + \sum_{i \neq j} \frac{P}{K}\left|\mathbf{h}_i^H \mathbf{v}_j\right|^2} = \frac{\frac{P}{K}\left|\mathbf{h}_i\right|^2 \left|\tilde{\mathbf{h}}_i^H \mathbf{v}_i\right|^2}{\sigma^2 + \left|\mathbf{h}_i\right|^2 \sum_{i \neq j} \frac{P}{K}\left|\tilde{\mathbf{h}}_i^H \mathbf{v}_j\right|^2}$$

will be analyzed separately.

4.1.3 Discussions of Interferences and Precoding Gain

a. Interferences

Fig. 4-3 shows the geometric representation of interferences where Ω is the angle between $\mathbf{v}_j$ and $\tilde{\mathbf{h}}_i$. The interferences for user i result from $\left|\tilde{\mathbf{h}}_i \mathbf{v}_j\right|^2$ for all $j \neq i$. Define

$$\left|\tilde{\mathbf{h}}_i^H \mathbf{v}_j\right|^2 = \cos^2 \Omega, \text{ for } i \neq j. \tag{4.1}$$

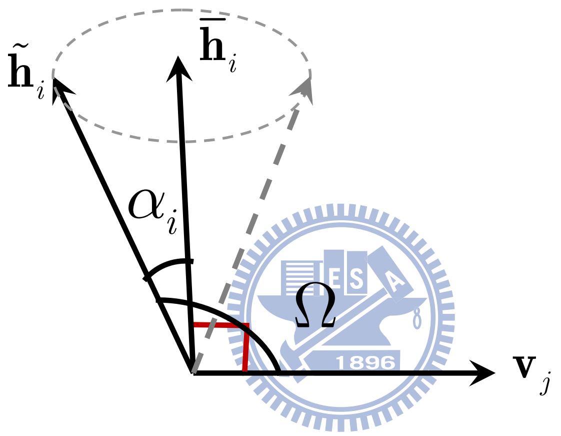

Fig. 4-3 Geometric representation of interference

From the assumption that $\alpha_i < \frac{\pi}{2}$, Ω is bounded by

$$\frac{\pi}{2} - \alpha_i \leq \Omega \leq \frac{\pi}{2} + \alpha_i. \tag{4.2}$$

So $\cos^2 \Omega \leq \sin^2 \alpha_i$, and the interferences have the upper bound as

$$\left|\tilde{\mathbf{h}}_i^H \mathbf{v}_j\right|^2 \leq \sin^2 \alpha_i. \tag{4.3}$$

From (4.3), we can conclude that the interferences for user i is only bounded by the sine of its own quantization angular error α_i and independent of other users' quantization errors.

b. Precoding Gain

As for the precoding gain, its geometrical representation is illustrated in **Fig. 4-4**. Now Ω is the angle between $\mathbf{v}_i$ and $\tilde{\mathbf{h}}_i$. The precoding gain for user i is $\left|\tilde{\mathbf{h}}_i^H \mathbf{v}_i\right|^2 = \cos^2 \Omega$.

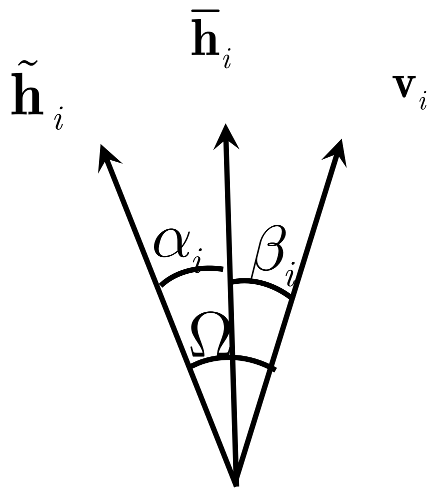

Fig. 4-4 Geometric representation of precoding gain

From the assumption that β_i is small and $\alpha_i + \beta_i < \frac{\pi}{2}$, we can infer that

$$\Omega \leq \alpha_i + \beta_i. \tag{4.4}$$

So $\cos^2 \Omega \geq \cos^2(\alpha_i + \beta_i) \approx \cos^2 \alpha_i$, and the precoding gain of user i has a lower bound as

$$\left|\tilde{\mathbf{h}}_i^H \mathbf{v}_i\right|^2 \geq \cos^2 \alpha_i. \tag{4.5}$$

Similar to the upper bound of interferences, we can conclude that the precoding gain of user i is only bounded by the cosine of its own quantization angular error α_i and independent of other users' quantization errors.

4.1.4 Conclusions

From above analysis of interferences and precoding gain, we can derive the lower bound of SINR as

$$\mathrm{SINR}_i = \frac{\frac{P}{K}\left|\mathbf{h}_i^H \mathbf{v}_i\right|^2}{\sigma^2 + \sum_{i \neq j} \frac{P}{K}\left|\mathbf{h}_i^H \mathbf{v}_j\right|^2} = \frac{\frac{P}{K}\left|\mathbf{h}_i\right|^2 \left|\tilde{\mathbf{h}}_i^H \mathbf{v}_i\right|^2}{\sigma^2 + \left|\mathbf{h}_i\right|^2 \sum_{i \neq j} \frac{P}{K}\left|\tilde{\mathbf{h}}_i^H \mathbf{v}_j\right|^2} \geq \frac{\frac{P}{K}\left|\mathbf{h}_i\right|^2 \cos^2\left(\alpha_i\right)}{\sigma^2 + \frac{P}{K}\left|\mathbf{h}_i\right|^2 \left(\sin^2 \alpha_i\right)(K-1)}. \tag{4.6}$$

To sum up, the lower bound of SINR for user i is only related to its own quantized angular error and independent of other users'. Our analysis of SINR is consistent with the simulation results in **Fig. 4-1**. Only the mobile user with higher feedback overheads benefits, while other users' performances remain the same.

4.2 Proposed Diagonal-wise Vector Quantization for Spatial Correlation Matrix Feedback

Generally, the codebook design is mainly based on typical communication environments. However, it is impossible to consider all cases. So, channel spatial correlation at the transmitter end can provide the current statistic information of the channel and therefore can be used to refine the codewords of the codebook, such that the refined codewords are more suitable for the current communication scenario. Methods of refining the codebook by using the channel spatial correlation can be found in [28]. In [28], the average spatial correlation matrix as defined in (4.7) is fed back to the transmitter. The average spatial correlation matrix is

$$\mathbf{R}_n = \frac{1}{T \times L} \sum_{t=1}^{T} \sum_{l=1}^{L} \mathbf{H}_{n \times T+t,l}^{H} \mathbf{H}_{n \times T+t,l}, \tag{4.7}$$

where t is time index, l is subcarrier index and n means to take average over n th time slot. Since the spatial correlation matrix $\mathbf{R}$ is a Hermitian matrix, we need only quantizing the upper triangular part of $\mathbf{R}$.

In the following sections, the spatially and temporally correlated channel model is given first, followed by the introduction of one of the existing methods for spatial correlation matrix feedback: entry-wise differential scalar quantization [29]. Finally, the proposed a diagonal-wise vector quantization scheme which feeds back spatial correlation matrix by exploiting the spatial correlation of channels is presented.

4.2.1 Correlated Channel Model [30]

The temporally correlated channel model used in Chapter 3 is modified to a spatially and temporally correlated channel model for the following sections. The new correlated channel model is

$$\mathbf{H}_{s,t} = unvec\left\{\mathbf{R}_s^{1/2} vec\left(\mathbf{H}_t\right)\right\}, \tag{4.8}$$

where the parameters are defined in **Table 4-4**. Generally, the temporal correlated channel is multiplied by the channel spatial correlation matrix $\mathbf{R}_s$ and become a spatially and temporally correlated channel.

Table 4-4 Parameter definitions

Parameters/functions	Definitions
$vec(.)$	Colum-wise stacking
$unvec(.)$	Reverse operation of $vec(.)$
$\mathbf{H}_t$	Temporally correlated channel defined in 2.3
$\mathbf{H}_{s,t}$	Spatially and temporally correlated channel
$\mathbf{R}_s$	$\mathbf{R}_s = \mathbf{R}_{BS} \otimes \mathbf{R}_{MS}$ ($\otimes$ is Kronecker product)

$\mathbf{R}_{BS}$ and $\mathbf{R}_{MS}$ in **Table 4-4** are the spatial correlation seen from BS and MS. Their corresponding (p,q) entries, $\left\{\mathbf{R}_{BS}\right\}_{pq}$ and $\left\{\mathbf{R}_{MS}\right\}_{pq}$, represent the antenna spatial correlation between the pth and qth antennas at the BS and MS respectively and are approximated using 20 subpaths as [30]

$$\begin{aligned} r_{BS}(p,q) &= \frac{1}{20}\sum_{k=1}^{20}\exp\left\{j\frac{2\pi d_{BS}}{\lambda}(p-q)\sin\left(AOD+\psi_{k,BS}+\theta_{BS}\right)\right\} \\ r_{MS}(p,q) &= \frac{1}{20}\sum_{k=1}^{20}\exp\left\{j\frac{2\pi d_{MS}}{\lambda}(p-q)\sin\left(AOA+\psi_{k,MS}+\theta_{MS}\right)\right\} \end{aligned}, \tag{4.9}$$

where d_{BS} and d_{MS} are the antenna spacings at BS and MS and λ is the wavelength. As we can see in **Fig. 4-5**, AOA_n and AOD_n are angles of arrival and departure for cluster n. The LOS directions with respect to the BS and MS are θ_{BS}

and θ_{MS} respectively. The angular offsets of k th subpath are determined by

$$\begin{aligned} \psi_{k,BS} &= \Delta_k \times AS_{BS} \\ \psi_{k,MS} &= \Delta_k \times AS_{MS}. \end{aligned} \tag{4.10}$$

AS_{BS} and AS_{MS} are cluster angular spreads. The values of Δ_k are shown in **Table 4-5**.

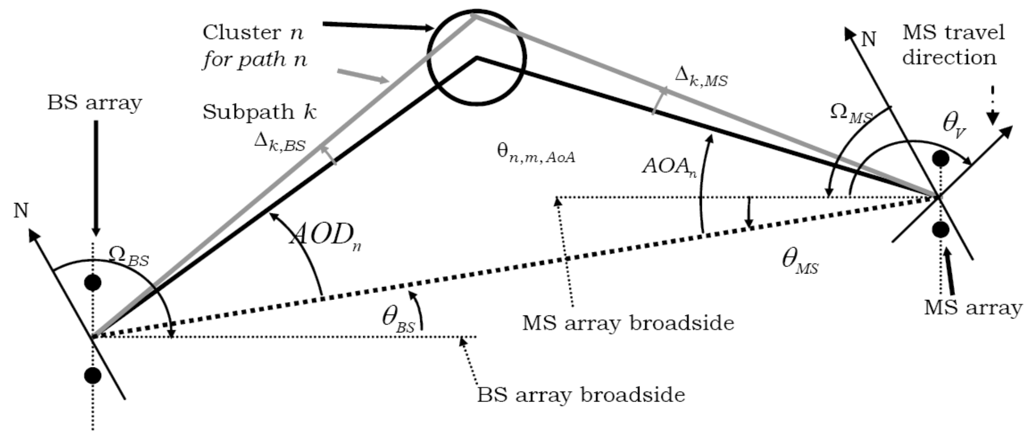

Fig. 4-5 Angle parameters in MIMO channel model [30]

Table 4-5 Values of Δ_k [30]

Sub-path number k	Δ_k
1,2	± 0.0447
3,4	± 0.1413
5,6	± 0.2492
7,8	± 0.3715
9,10	± 0.5129
11,12	± 0.6797
13,14	± 0.8844
15,16	± 1.1481
17,18	± 1.5195
9,20	± 2.1551

From (4.9), we can determine $\mathbf{R}_{BS}$ and $\mathbf{R}_{MS}$, and once $\mathbf{R}_{BS}$ and $\mathbf{R}_{MS}$ are known, the spatially and temporally correlated channel can be determined by multiplying the original temporally correlated with spatial correlation $\mathbf{R}_s$.

4.2.2 Existing Solution: Entry-wise Differential Scalar Quantization [29]

The basic idea of entry-wise differential scalar quantization is to quantize differential spatial correlation matrix $\left(\mathbf{R}_n - \bar{\mathbf{R}}_{n-1}\right)$ entry-wise. The mathematical representation to update the quantized spatial correlation matrix at the transmitter end is

$$\bar{\mathbf{R}}_n = \gamma \bar{\mathbf{R}}_{n-1} + \mathbf{C}_n, \tag{4.11}$$

where $\bar{\mathbf{R}}_n$ is the quantized matrix at time slot n, $\mathbf{C}_n$ is the differential updating matrix, and γ is forgetting factor. The elements of $\mathbf{C}_n$ are determined by the difference of current matrix $\mathbf{R}_n$ and previous quantized matrix $\bar{\mathbf{R}}_{n-1}$ (i.e., $\mathbf{R}_n - \bar{\mathbf{R}}_{n-1}$). The real and imaginary parts of each entry in $\mathbf{C}_n$ are individually quantized. Since the entries in the main diagonal of $\mathbf{R}_n$ are all real, the number of quantization bits is half for the main diagonal entries compared to those off-diagonal entries. The main diagonal entries are quantized as follows

$$\{\mathbf{C}_n\}_{pp} = \Delta \times \operatorname{sgn}\left(\{\mathbf{R}_n\}_{pp} - \gamma\left\{\bar{\mathbf{R}}_{n-1}\right\}_{pp}\right), \tag{4.12}$$

where Δ is stepsize. As for the complex off-diagonal entries ($q > p$)

$$\begin{aligned}\{\mathbf{C}_n\}_{pq} = {} & \Delta \times \operatorname{sgn}\left(\operatorname{Re}\left\{\{\mathbf{R}_n\}_{pq}\right\} - \operatorname{Re}\left\{\gamma\{\mathbf{R}_n\}_{pq}\right\}\right) \\ & + j\Delta \times \operatorname{sgn}\left(\operatorname{Im}\left\{\{\mathbf{R}_n\}_{pq}\right\} - \operatorname{Im}\left\{\gamma\{\mathbf{R}_n\}_{pq}\right\}\right).\end{aligned} \tag{4.13}$$

Entry-wise differential SQ uses 4 bits per real/imaginary component for the initial full quantization while 1 bits per real/imaginary component for differential quantization. The differential quantization scheme is mainly to exploit temporal correlation of the channel. In the next section, we propose another method to quantize the spatial correlation matrix $\mathbf{R}_n$ more effectively.

4.2.3 Proposed Diagonal-wise Full Vector Quantization

The quantization scheme proposed in 4.2.2 requires a large number of bits since it is an entry-wise quantization method. Our first attempt to quantize the spatial correlation matrix is column-wisely vector quantization as shown in **Fig. 4-6**, but the result is not very effective.

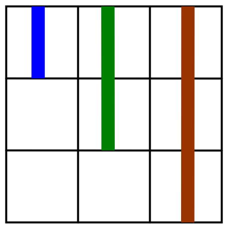

Fig. 4-6 column wise vector quantization

We further investigate the structure of the spatial correlation matrix,

$$\mathbf{R}_n = \frac{1}{T \times L}\sum_{t=1}^{T}\sum_{l=1}^{L}\begin{bmatrix}\mathbf{h}_{1,t',l} & \mathbf{h}_{2,t',l} & \cdots & \mathbf{h}_{K,t',l}\end{bmatrix}^H \begin{bmatrix}\mathbf{h}_{1,t',l} & \mathbf{h}_{2,t',l} & \cdots & \mathbf{h}_{K,t',l}\end{bmatrix}, \tag{4.14}$$

where $t' = T \times (n-1) + t$. It is not difficult to observe that $[\mathbf{R}_n]_{i,j}$ reflects the average spatial correlation between two channel vectors $\mathbf{h}_i$ and $\mathbf{h}_j$. As $|i-j|$ increases, the magnitude of $[\mathbf{R}_n]_{i,j}$ decreases, which means when the ith and jth antennas at MS are located far away, the spatial correlation is smaller. So as one moves from the main diagonal to the top off-diagonal, the magnitudes of the entries will decrease. Putting those entries which have similar magnitude together as a vector, we propose diagonal-wise full vector quantization as shown in **Fig. 4-7**.

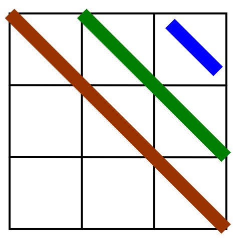

Fig. 4-7 Diagonal-wise full vector quantization

The proposed scheme can successfully exploit the property of spatial correlation matrix that the diagonal entries have similar magnitudes and hence it can quantize the matrix effectively with a lower cost of feedback overhead. Take a 3×3 spatial correlation matrix as example, the system requires three sets of codebooks which are trained by GLA separately. The bit allocation for each codebook can be further optimized, but in our simulation, we simply allocate more bits for the vector which has more real variables.

Also, the number of quantization bits of the proposed method can be further reduced by decreasing the feedback frequency as shown in **Fig. 4-8**. Only the first matrix in the N matrices sequence is quantized and fed back, and the remaining $N-1$ time slots use the first quantized matrix at the transmitter end.

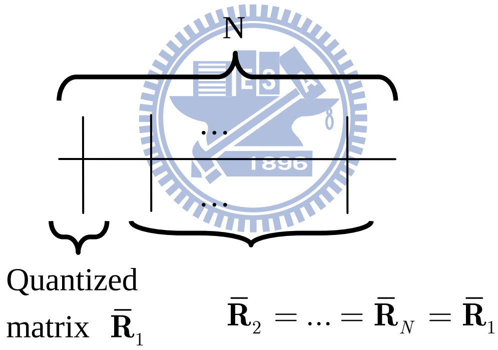

Fig. 4-8 Reducing the feedback frequency

4.2.4 Comparisons Between Entry-wise Differential SQ and Proposed Diagonal-wise Full VQ

Before the demonstration of computer simulations, we compare the number of quantization bits between entry-wise differential SQ and the proposed diagonal-wise VQ. In our simulation environment, the system is 3×3 MIMO. We allocate 5, 6, and 3 bits for the three codebooks respectively to make the largest average quantization bit (when $N=1$) for a matrix to be 14 bits which is still smaller than the average quantization bits (14.4 bits) for entry-wise differential SQ.

Table 4-6 Comparisons of diagonal-wise full VQ and enty-wise differential SQ

<table>
<tr><td></td><td>Diagonal-wise Full VQ</td><td>Entry-wise Differential SQ</td></tr>
<tr><td>Number of bits for full quantization</td><td>Total: 14 bits
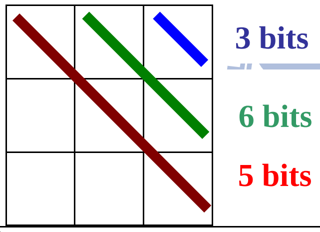</td><td>Total: 36 bits<table><tr><td>4</td><td>8</td><td>8</td></tr><tr><td></td><td>4</td><td>8</td></tr><tr><td></td><td></td><td>4</td></tr></table></td></tr>
<tr><td>Number of bits for differential quantization</td><td></td><td>Total: 9 bits<table><tr><td>1</td><td>2</td><td>2</td></tr><tr><td></td><td>1</td><td>2</td></tr><tr><td></td><td></td><td>1</td></tr></table></td></tr>
<tr><td></td><td>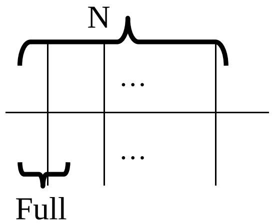
Average: $\frac{14}{N}$ bits</td><td>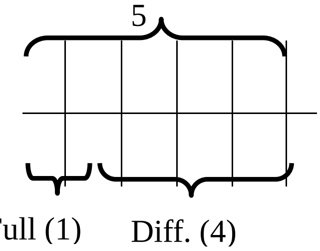
Average: $\frac{36\times1+9\times4}{5}=14.4$ bits</td></tr>
</table>

4.2.5 Computer simulations

In this section, the computer simulations are based on two different environments: time-invariant channel and time-varying channel. For time-varying channel, the angle of departure and arrival (AOD and AOA) related to the spatial correlation of channel shown in (4.9) is updated every 0.1 second according to a linear equation

$$
\begin{aligned}
AOD_m &= AOD_{m-1} + 2^\circ \\
AOA_m &= AOA_{m-1} + 2^\circ
\end{aligned}
\tag{4.15}
$$

where m is time index and the initial AOD and AOA are $AOD_0 = 0^\circ$, $AOA_0 = 0^\circ$. As for the time- invariant channel, the AOD and AOA remain unchanged all the time ($AOD = 0^\circ$, $AOA = 0^\circ$).

The following simulations consider 3×3 MIMO OFDM systems. The simulation parameters are listed in **Table 4-7**. At the receiver end, the CSI is estimated every 1 ms. The fed back average spatial correlation is

$$
\mathbf{R}_n = \frac{1}{40 \times 48} \sum_{t=1}^{40} \sum_{k=1}^{48} \mathbf{H}_{t',l}^H \mathbf{H}_{t',l},\ t' = 40(n-1) + t \tag{4.16}
$$

which takes average over 40 ms and 48 subcarriers. Our performance metric is the normalized MSE as follows

$$
E\left[\frac{\left\| \overline{\mathbf{R}}_n - \mathbf{R}_n \right\|_F^2}{\left\| \mathbf{R}_n \right\|_F^2} \right] \tag{4.17}
$$

where $\overline{\mathbf{R}}_n$ is the quantized matrix.

Table 4-7 Simulation parameters

Parameters	**value**					
Channel	Multipath Rayleigh fading channel					
Tap	1	2	3	4	5	6
Relative delays (ms)	0	10	20	30	40	50
Spatial correlation parameters	$AS_{BS} = 10^\circ$, $AS_{MS} = 22^\circ$, $\theta_{BS} = 0^\circ$, $\theta_{MS} = 0^\circ$					
Antenna spacing	$\lambda / 2 = f_c / (2 \times c)$, $c = 3 \times 10^8$					
Number of transmit antennas	3					
Number of receive antennas	3					
N	1-3					
Sampling time	1 ms					
Number of subcarriers	512					
Carrier frequency f_c	2.5 G Hz					
Codebooks **for diagonal-wise full VQ**	For time-invarying channel environment: **Table 4-8**, **Table 4-9**, **Table 4-10** For time-varying channel environment: **Table 4-11**, **Table 4-12**, **Table 4-13**					
Forgeting factor γ **and stepsize** α **for entry-wise differential SQ**	$\gamma = 0.98$ $\alpha = 5$					

Table 4-8 Codebooks for third diagonal (1×1 vector) under time-invariant channel environment

Index	1	2	3	4	5	6	7	8
5 km/hr	8.194+ 5.667i	28.433- 2.329i	15.012- 7.541i	5.212- 5.058i	2.655+ 0.878i	18.540 + 8.975i	8.949 - 0.631i	15.709+ 0.64i
15 km/hr	4.316- 1.607i	11.386+ 4.544i	19.845+ 3.357i	5.246+ 2.839i	8.600+ 0.133i	13.345- 0.301i	17.618- 4.862i	9.403- 4.528i
30 km/hr	9.575 - 3.772i	16.297- 2.86i	12.070- 0.421i	15.930+ 2.822i	5.173- 1.481i	10.247+ 3.118i	8.444 - 0.243i	5.887+2.057i
50 km/hr	9.346- 2.949i	14.535- 2.337i	6.480+ 1.891i	5.689- 1.086i	10.148+0.685i	11.404- 0.303i	14.657+ 2.052i	8.518- 0.073i

Table 4-9 Codebooks for secondary diagonal (2×1 vector) under time-invariant channel environment

	Codewords for 5 km/hr		Codewords for 15 km/hr		Codewords for 30 km/hr		Codewords for 50 km/hr	
1	9.436 + 2.573i	7.783 + 2.421i	9.212 - 0.245i	10.624 - 0.449i	14.790 + 0.06i	12.594 - 0.009i	12.576 + 0.488i	12.188 + 0.701i
2	36.895 - 1.321i	24.665 - 1.614i	13.662 + 1.287i	13.227 + 1.176i	23.085 - 1.125i	27.584 - 1.204i	15.5 - 0.133i	20.565 - 0.05i
3	28.749 - 5.436i	17.56 - 5.096i	35.434 + 1.239i	28.924 + 0.908i	11.673 + 0.887i	14.542 + 1.05i	14.899 + 0.668i	14.294 + 0.856i
4	16.613 - 3.253i	9.461 - 3.115i	12.637 + 3.056i	12.11 + 3.152i	23.138 + 2.575i	25.006 + 2.692i	13.291 - 0.663i	10.881 - 0.596i
5	23.386 - 1.424i	13.243 - 0.997i	18.125 - 1.451i	19.752 - 1.496i	10.636 - 0.125i	12.44 - 0.159i	17.507 + 2.493i	16.6 + 2.355i
6	20.814 + 6.667i	20.159 + 6.669i	23.264 - 0.829i	14.74 - 0.991i	18.772 + 2.665i	17.457 + 2.656i	18.052 + 0.744i	13.759 + 0.716i
7	9.715 + 4.013i	12.105 + 4.011i	28.438 - 2.764i	20.87 - 2.708i	12.095 - 1.795i	16.57 - 1.649i	16.363 + 0.854i	16.079 + 0.961i
8	14.27 + 4.234i	20.378 + 4.171i	18.538 - 2.687i	13.515 - 2.578i	16.1 + 2.265i	14.901 + 2.38i	20.238 + 1.408i	16.542 + 1.474i
9	12.286 + 1.35i	12.167 + 1.372i	18.594 - 4.206i	17.539 - 4.041i	20.262 - 0.473i	20.8 - 0.367i	16.145 + 2.117i	14.07 + 1.954i
10	5.496 + 2.014i	8.068 + 2.044i	11.444 + 2.803i	15.923 + 2.641i	13.598 + 1.332i	11.03 + 1.203i	13.612 + 0.996i	10.642 + 0.881i
11	5.074 - 0.25i	9.59 - 0.197i	22.839 + 3.477i	19.683 + 3.562i	20.556 - 1.414i	15.362 - 1.475i	15.217 + 1.524i	18.182 + 1.639i
12	6.575 + 0.533i	14.116 + 0.513i	27.613 + 3.165i	30.25 + 2.878i	12.654 + 0.134i	13.02 + 0.026i	15.780 + 0.824i	11.968 + 1.089i
13	29.447 - 0.603i	30.928 - 0.501i	19.566 - 0.525i	16.546 - 0.82i	18.082 + 0.71i	19.631 + 0.442i	25.891 - 1.003i	21.954 - 1.105i
14	15.649 - 0.455i	6.999 - 0.318i	16.194 + 0.841i	22.999 + 0.666i	12.934+ 2.614i	16.469 + 2.535i	23.335 + 1.397i	22.522 + 1.539i
15	7.822 + 0.122i	7.376 + 0.077i	7.792 - 0.111i	12.968 - 0.1i	8.287 - 0.055i	11.958 - 0.192i	17.987+ 0.826i	18.037 + 0.987i
16	5.972 - 1.98i	7.306 - 1.9i	14.188 - 2.781i	11.519 - 2.719i	16.174 + 0.798i	17.536 + 0.991i	19.728 - 0.33i	18.033 - 0.381i
17	16.18 + 0.09i	11.56 - 0.168i	13.715 - 3.429i	15.272 - 3.349i	30.587 + 0.134i	30.204 + 0.134i	8.117 - 0.249i	9.373 - 0.273i
18	11.747 + 0.03i	8.939 + 0.099i	11.27 - 1.646i	8.23 - 1.631i	10.156 - 0.558i	14.984 - 0.399i	11.889+ 0.212i	9.26 + 0.236i
19	37.39 + 4.75i	31.57 + 4.66i	22.142 - 1i	29.726 - 1.215i	17.525 - 2.841i	16.296 - 2.898i	13.771 + 1.946i	15.74 + 1.798i
20	7.63 - 1.139i	4.553 - 1.299i	18.989 + 0.135i	11.817 + 0.071i	10.744 - 1.599i	9.185 - 1.518i	13.209 + 0.327i	17.994 + 0.167i
21	19.648 + 2.461i	17.359 + 2.373i	8.114 - 0.986i	6.38 - 1.024i	24.022 + 1.131i	19.329 + 1.263i	12.059 - 0.239i	12.52 - 0.508i
22	60.339 - 6.691i	52.374 - 8.42i	14.825 + 0.03i	11.485 + 0.148i	15.612 - 0.695i	20.986 - 0.708i	16.063 - 0.178i	17.971 - 0.149i
23	28.848 - 6.853i	30.171 - 6.755i	8.648 + 2.192i	12.072+ 2.144i	14.923 + 0.123i	14.68 + 0.156i	14.686 - 0.691i	14.675 - 0.653i
24	22.066 - 4.218i	25.686 - 4.018i	13.065 + 1.228i	19.598 + 1.402i	18.362 - 1.563i	18.713 - 1.379i	15.759 - 0.542i	11.124 - 0.603i
25	20.061 - 5.101i	14.827 - 5.436i	13.058 - 0.75i	13.964 - 0.744i	25.787 - 3.037i	23.676 - 2.785i	13.19 + 0.65i	14.174 + 0.457i
26	24.038 + 2.262i	20.894 + 2.361i	16.702 + 0.372i	14.518 + 0.524i	18.357 + 0.521i	23.899 + 0.174i	14.007 + 1.643i	12.903 + 1.479i
27	16.093 + 1.3i	26.126 + 1.901i	11.58 + 0.798i	6.594 + 0.917i	16.836 + 0.421i	14.863 + 0.535i	17.997 - 1.547i	21.916 - 1.699i

28	15.182 + 5.275i	13.858 + 5.425i	22.352 - 3.128i	19.568 - 2.989i	19.607 + 1.278i	14.527+ 1.247i	17.972 - 0.251i	16.097 - 0.009i
29	27.492 + 3.585i	38.508 + 3.561i	10.166 - 2.14i	14.792 - 2.311i	22.811 - 2.096i	19.005 - 1.903i	23.269+ 0.444i	19.045 + 0.359i
30	20.376 + 2.207i	10.853 + 2.24i	19.641 + 3.061i	25.831 + 2.59i	15.242 - 0.54i	10.431- 0.484i	16.131 - 0.014i	14.049 - 0.101i
31	15.814 - 2.791i	18.737 - 2.927i	24.365 + 1.876i	24.51 + 2.223i	16.036 - 2.484i	12.6 - 2.417i	19.14 + 0.963i	22.709 + 0.869i
32	22.999 + 0.396i	27.327 + 0.843i	35.449 + 1.984i	40.205 + 2.309i	8.13 - 0.726i	9.46 - 0.732i	20.216 - 0.896i	15.393 - 0.893i
33	15.864 + 2.297i	14.389 + 2.206i	19.665 + 1.262i	20.042 + 1.09i	11.236 + 0.875i	11.538 + 1.032i	26.072 + 0.475i	27.015 + 0.738i
34	43.255 - 3.39i	35.598 - 3.304i	15.537 + 2.777i	15.705 + 2.915i	9.562 + 1.508i	13.611 + 1.506i	20.63 + 1.206i	20.006 + 1.272i
35	19.162 - 0.18i	21.974 - 0.279i	6.92 + 0.584i	9.277+ 0.642i	6.717 - 0.056i	7.278 + 0.018i	15.491 - 1.969i	18.872 - 1.98i
36	32.921 - 4.52i	42.891 - 3.873i	7.863 + 0.917i	6.891 + 0.982i	12.618 - 0.276i	11.141 - 0.325i	14.42 + 0.389i	16.157 + 0.401i
37	15.405 - 2.937i	14.186 - 2.802i	17.714 - 2.845i	23.900- 3.048i	15.201 - 2.032i	18.332 - 1.994i	14.153 + 0.014i	12.653 - 0.043i
38	11.201 + 2.169i	16.058 + 2.012i	23.672 + 0.14i	19.617 - 0.092i	9.766 - 0.461i	7.57 - 0.426i	18.148 - 1.983i	17.411 - 1.908i
39	8.878 - 1.012i	9.985 - 1.202i	21.286 - 0.711i	23.267 - 0.689i	11.834 - 1.481i	13.443 - 1.432i	21.205- 1.701i	19.898 - 1.725i
40	7.13 + 1.395i	4.644 + 1.353i	28.564 + 2.12i	20.548+ 2.214i	19.347 - 2.834i	21.833- 3.081i	18.1 - 0.287i	19.822 - 0.374i
41	22.347 - 1.65i	18.725 - 1.807i	7.18 - 1.644i	9.145 - 1.52i	14.223 - 1.247i	13.077 - 1.155i	11.44 - 1.321i	10.881 - 1.166i
42	42.577 + 5.101i	47.644 + 5.662i	11.74 - 1.123i	17.598 - 1.282i	15.012 - 0.589i	16.925 - 0.562i	9.578 - 0.775i	11.807 - 0.741i
43	8.837 + 0.851i	20.141+ 1.035i	5.345 + 0.108i	6.065 + 0.11i	15.735 + 2.228i	19.833+ 2.318i	13.01 - 1.948i	14.766 - 2.066i
44	10.783 - 2.138i	17.587 - 2.355i	16.62 + 0.674i	17.948 + 0.505i	20.244 + 2.295i	20.979 + 2.351i	13.126 - 0.723i	13.696 - 0.584i
45	4.228 - 0.007i	4.761 - 0.069i	13.835 + 0.669i	16.154 + 0.612i	27.573 + 0.758i	23.747 + 0.858i	14.085 - 1.194i	16.727 - 1.133i
46	10.942 + 0.341i	5.557 + 0.417i	10.998 + 0.871i	12.073 + 0.889i	17.885 - 0.279i	16.671 - 0.322i	9.1 + 0.769i	11.262 + 0.797i
47	20.094 + 6.109i	28.697 + 5.871i	15.5 - 1.544i	16.62 - 1.606i	16.287 + 1.294i	12.091+ 1.357i	12.348 - 0.376i	15.565 - 0.478i
48	8.666 + 1.098i	11.152+ 1.121i	23.184 - 4.331i	24.527 - 4.61i	22.699 - 0.297i	22.893 - 0.617i	8.003 - 0.084i	7.338 - 0.093i
49	12.972 - 2.433i	23.57 - 1.939i	9.982 + 1.935i	9.21 + 1.948i	13.503 - 2.856i	14.546- 2.806i	11.301 + 0.139i	11.085 + 0.057i
50	24.237 + 4.466i	14.543 + 4.319i	12.148 + 0.449i	9.807 + 0.429i	17.944 - 0.727i	13.178 - 0.721i	10.435 - 1.028i	8.935 - 1.059i
51	27.6 - 1.261i	23.324 - 1.194i	9.539 - 0.132i	8.462 - 0.033i	15.721 - 1.308i	15.002 - 1.413i	11.957 + 1.695i	13.268 + 1.706i
52	18.633 - 0.546i	15.353 - 0.54i	30.955 - 4.192i	31.526 - 3.114i	12.457 - 0.34i	8.908 - 0.21i	11.069 - 1.031i	13.855 - 1.002i
53	13.874 - 0.408i	15.318 - 0.444i	10.396 + 0.657i	15.14 + 0.418i	11.442 + 1.452i	9.197+ 1.332i	15.682 - 2.228i	15.199 - 2.251i
54	12.042 - 5.239i	13.75 - 5.205i	10.419 - 1.009i	12.745- 0.986i	12.066 + 2.397i	12.362 + 2.441i	9.992 - 0.209i	10.163 - 0.171i
55	19.772 - 0.821i	34.115 - 1.195i	10.432 - 2.707i	11.061 - 2.709i	8.984 + 0.884i	8.207 + 0.848i	10.624 + 0.43i	13.199 + 0.414i
56	10.895 - 2.639i	7.372 - 2.654i	15.809 - 1.297i	13.381 - 1.4i	10.362 - 0.212i	10.165- 0.127i	14.895 - 1.352i	12.901 - 1.36i
57	17.796 - 5.954i	21.908 - 6.079i	27.712 - 1.085i	25.785 - 1.513i	13.851 + 1.471i	13.768 + 1.518i	17.462 - 1.36i	13.879 - 1.142i
58	28.369 + 5.285i	25.34 + 5.227i	20.368 + 2.139i	15.81 + 2.092i	12.783 + 0.209i	18.342 + 0.225i	11.219 + 1.404i	11.024+ 1.458i
59	10.442 - 0.816i	13.667 - 0.924i	12.071 - 0.955i	11.046 - 1.101i	12.987 - 0.547i	15.106 - 0.639i	16.155 - 0.659i	16.123 - 0.856i
60	29.94 + 1.732i	16.737 + 0.983i	17.287 + 2.578i	12.46 + 2.462i	20.673 + 0.342i	17.6 + 0.399i	9.708 + 0.964i	8.725 + 0.972i
61	14.241 + 2.758i	8.806 + 2.699i	14.285 - 1.909i	20.103 - 2.095i	10.027 - 1.616i	11.707 - 1.673i	12.778 - 1.785i	12.252 - 1.884i
62	15.206 + 0.755i	19.202 + 0.444i	14.895 - 0.691i	8.540- 0.725i	12.713- 1.887i	11.102 - 1.825i	11.608 + 0.757i	15.282 + 0.942i
63	12.624 - 1.957i	11.128 - 1.778i	14.219 + 2.089i	9.619 + 1.806i	8.957 + 1.297i	10.518 + 1.244i	17.92 + 2.167i	20.064 + 2.263i
64	7.86 - 3.143i	12.096 - 2.948i	17.319 + 3.727i	19.402 + 3.523i	13.973 + 0.996i	16.141+ 0.971i	21.555 - 1.186i	23.951 - 1.417i

Table 4-10 Codebooks for main diagonal (3×1 vector) under time-invariant channel environment

	Codewords for 5 km/hr			Codewords for 15 km/hr			Codewords for 30 km/hr			Codewords for 50 km/hr		
1	15.15	9.95	7.98	9.43	11.62	16	15.43	16.96	15.97	11.32	13.14	16.6
2	41.5	30.03	18.05	13.85	16.18	16.42	23.29	29.97	32.26	16.09	20.96	25.49
3	34.85	36.72	29.26	37.88	35.91	26.46	15.01	14.46	17.31	13.33	13.6	15.07
4	20.36	15.78	16.87	15.42	14.03	12.65	25.31	27.2	25.47	16.82	13.49	11.11
5	34.49	21.9	12.07	16.75	19.66	19.09	10.36	11.36	13.89	18.24	18.75	19.41
6	22.73	24.1	22.72	28.83	21.45	14.61	18.93	20.38	20.52	21.58	18.12	14.72
7	10.5	17.7	29.18	34.33	27.85	18.24	12.43	15.21	17.51	16.73	17.95	16.89
8	14.54	17.11	16.31	23.18	19.07	15.3	16.53	14.69	13.75	22.49	20.53	17.73
9	10.83	15.95	20.85	20.45	19.27	20.84	22.13	21.79	19.26	18.26	16.94	14.69
10	10.92	7.56	6.83	11.85	17.43	25.45	19.19	14.36	11.2	14.55	13.18	13.07
11	6.77	6.33	7.95	21.33	24.09	22.73	26.19	21.27	15.95	20.29	25.21	28.18
12	7.52	11.08	20.06	28.26	32.14	30.14	13.38	13.59	14.48	19.31	17.08	17.01
13	26.44	36.81	38.72	21.35	22.01	17.93	20.24	22.9	23.52	28.84	26.14	20.56
14	20.7	12.19	8.65	15.54	23.08	30.93	12.13	15.91	21.68	27.16	29.41	27.42
15	10.8	10.25	10.61	8.32	8.96	12.09	10.4	12.71	17.25	17.12	19.92	21.5
16	7.38	8.67	13.45	19.47	15.5	13.15	14.68	17.6	19.48	20.47	21.29	20.41
17	15.16	19.36	22.51	16.63	21.23	24.47	32.72	32.91	26.96	10.69	9.75	10.67
18	13.79	11.94	16.68	14.58	10.58	9.29	15.88	19.51	22.59	13.67	11.58	10.92
19	49.62	43.35	27.65	21.18	30.41	36.36	21.8	19.14	16.59	15.46	17.34	19.2
20	15.34	13.69	11.62	24.17	16.4	11.08	12.69	11.69	11.98	12.83	15.52	19.68
21	17.02	23.87	27.06	9.84	8.03	8.42	24.81	24.36	20.84	11.44	11.69	13.54
22	61.72	64.37	46.56	18.48	17.98	15.49	19.21	24.77	28.45	14.11	18	22.17
23	35.28	48.73	48.8	11.69	11.04	11.68	17.55	17.37	19.13	16.51	15.54	16.71
24	29.66	28.56	21.01	14.41	17.32	21.09	18.59	19.28	17.14	20.41	15.63	12.31
25	26.18	22.14	16.07	12.83	12.84	14.86	30.24	26.45	20	13.88	15.45	17.11
26	19.24	21.46	18.04	16.96	15.04	17.29	14.81	20.8	26.43	15.15	15.36	14.73
27	15.8	26.24	36.02	18.67	12.74	9.84	18.28	16.05	16.08	19.65	22.37	23.62
28	10.26	13.2	14.62	26.14	23.84	19.49	23.11	17.35	12.89	19.68	19.59	17.43
29	18.03	34.52	49.71	11.13	14.16	19.7	19.36	17.3	13.93	24.26	23.08	19.78
30	26.07	16.51	10.82	27.73	28.21	23.72	13.94	10.57	9.4	17.23	14.78	13.72
31	19.68	17.8	12.29	21.75	26.32	27.95	15.66	12.91	11.47	23.34	24.76	23.24
32	23.91	30.14	29.16	33.71	41.1	40.85	9.89	9.04	10.27	25.57	20.34	15.49

Table 4-11 Codebooks for third diagonal (1×1 vector) under time-varying channel environment

Index	1	2	3	4	5	6	7	8
5 km/hr	-2.669 + 24.347i	-4.777 + 9.113i	1.047 + 3.543i	17.209 + 4.041i	13.029 + 18.56i	8.000 + 7.408i	6.736 - 0.133i	2.46 + 12.835i
15 km/hr	-3.008 + 10.97i	13.316 + 3.525i	0.46 + 5.233i	6.011 + 0.937i	7.097 + 6.451i	11.961 + 13.521i	1.176 + 19.095i	3.614 + 11.01i
30 km/hr	4.182 + 2.522i	14.122 + 4.809i	9.889 + 9.571i	4.924 + 6.995i	9.006 + 2.349i	3.766 + 12.349i	-0.388 + 7.449i	-2.458 + 13.383i
50 km/hr	3.076 + 8.668i	5.003 + 12.995i	-1.334 + 12.174i	4.676 + 4.528i	8.149 + 1.773i	12.528 + 4.301i	8.184 + 7.7i	-0.915 + 7.358i

Table 4-12 Codebooks for secondary diagonal (2×1 vector) under time-varying channel environment

	Codewords for 5 km/hr		Codewords for 15 km/hr		Codewords for 30 km/hr		Codewords for 50 km/hr	
1	12.196 + 3.611i	14.898 + 4.405i	12.623+ 3.732i	12.377 + 3.623i	9.348 + 0.697i	11.292 + 0.98i	13.106 + 2.715i	12.566 + 2.621i
2	3.635 + 3.246i	3.57 + 3.249i	20.738 - 0.134i	21.219 + 0.268i	24.114 + 3.23i	24.1 + 3.086i	22.154 + 8.92i	21.323 + 8.658i
3	7.269 + 5.074i	7.228 + 5.004i	10.433 + 1.137i	13.282 + 1.756i	18.069 + 4.633i	17.371 + 4.493i	16.309 + 5.763i	17.66 + 6.152i
4	28.434 + 6.156i	19.533 + 4.19i	18.521 + 1.193i	15.305 + 0.569i	19.454 + 2.446i	15.413 + 1.758i	12.175 + 1.688i	15.196 + 2.152i
5	17.088 + 5.909i	17.178 + 5.716i	14.608 + 1.086i	19.259 + 2.023i	15.456 - 0.195i	15.169 - 0.233i	15.355 + 0.684i	16.719 + 0.859i
6	11.839 + 2.377i	11.453 + 2.448i	28.564 + 9.852i	21.341 + 7.512i	14.842 + 6.2i	16.443 + 6.876i	21.421 + 2.619i	19.604 + 2.216i
7	5.323 + 2.069i	7.31 + 2.892i	21.747 + 8.621i	16.132 + 6.34i	7.648+ 1.406i	8.035 + 1.46i	15.244 + 2.92i	14.963+ 2.988i
8	11.021 + 4.968i	18.344 + 7.938i	21.931 + 7.173i	21.863 + 6.989i	14.194 + 6.917i	12.492 + 6.27i	8.022 + 2.906i	7.968 + 2.837i
9	14.4050+ 1.945i	20.928 + 3.969i	34.098 + 16.317i	31.643 + 15.044i	9.744 + 5.869i	8.212 + 5.018i	8.875 + 3.303i	10.514 + 3.905i
10	3.777 + 3.983i	7.446 + 6.606i	14.693 + 1.632i	11.1520 + 0.997i	16.008 + 8.243i	18.739 + 9.441i	10.828 + 4.981i	9.312 + 4.309i
11	13.635 + 11.147i	22.81 + 17.512i	8.49 + 7.035i	12.722 + 9.805i	6.095 + 4.428i	5.909 + 4.49i	15.174 + 10.775i	12.556 + 9.027i
12	19.137 + 12.027i	15.394 + 9.954i	15.627 + 10.74i	15.242 + 10.403i	13.658 + 9.963i	10.42 + 7.761i	15.787 + 12.702i	16.572 + 13.198i
13	10.779 + 6.021i	8.487 + 4.811i	7.776 + 1.961i	9.868 + 2.465i	6.442 + 8.228i	7.251 + 8.97i	9.794 + 5.062i	11.34 + 5.848i
14	21.496 + 26.532i	27.948 + 32.005i	8.925 + 7.579i	6.756 + 5.843i	7.140 + 6.890i	6.33 + 6.215i	12.548 + 8.334i	13.351 + 8.790i
15	21.649 + 14.001i	30.287 + 18.978i	12.217 + 10.826i	8.406 + 7.858i	12.518 + 10.684i	14.762 + 12.465i	8.358 + 5.124i	8.732 + 5.341i
16	15.719+ 19.259i	21.137 + 24.335i	11.494 + 5.561i	13.075+ 6.253i	9.561 + 9.758i	11.998+ 11.862i	9.785 + 8.452i	12.238 + 10.487i
17	20.672 + 25.862i	14.9 + 20.986i	11.249 + 15.085i	11.308 + 15.174i	14.574 + 13.311i	12.648 + 11.658i	10.436 + 7.391i	9.622 + 6.849i
18	9.172 + 12.618i	15.599 + 18.728i	14.305 + 13.573i	11.097 + 10.772i	17.716 + 11.676i	15.297 + 10.286i	8.024+ 7.057i	9.501 + 8.261i
19	8.126 + 10.32i	6.017 + 8.354i	4.915 + 5.194i	4.604 + 5.009i	7.383 + 9.955i	8.905 + 11.503i	10.689 + 11.811i	12.429 + 13.431i
20	12.602 + 19.851i	11.923 + 19.466i	12.928 + 15.658i	16.669 + 19.316i	12.292 + 15.393i	10.439 + 13.533i	11.831 + 11.982i	9.64 + 9.956i
21	21.466 + 1.145i	18.563 + 0.89i	14.562 + 2.612i	15.040+ 2.655i	14.89 + 2.25i	15.416 + 2.292i	16.779 + 5.235i	14.292 + 4.644i
22	17.856 + 0.874i	11.01 - 0.549i	13.787 - 0.771i	14.47 - 0.605i	11.261+ 1.451i	8.946 + 1i	17.962 + 3.658i	17.224 + 3.437i
23	13.031 + 3.19i	6.698 + 1.433i	18.879 + 3.31i	23.149 + 4.302i	22.728 + 5.444i	18.462 + 4.311i	20.395 + 5.85i	17.52 + 5.308i
24	16.287 + 2.828i	14.687 + 2.268i	17.684 + 4.172i	18.216 + 4.222i	12.088+ 2.553i	11.759 + 2.392i	10.581 + 1.107i	12.616 + 1.423i
25	7.226 + 6.474i	9.18 + 8.217i	24.463 + 12.754i	22.726 + 11.729i	13.286 + 0.283i	11.917 + 0.186i	18.131 + 1.298i	19.169 + 1.238i
26	21.393 + 6.589i	20.754 + 6.567i	17.283 + 7.641i	17.449 + 7.835i	9.641 + 3.138i	12.311 + 4.001i	17.887 + 9.212i	18.777 + 9.737i

27	11.856 - 0.816i	10.819 - 0.953i	22.986 + 3.736i	18.164 + 2.709i	13.530 + 3.616i	17.447 + 4.691i	14.198 + 4.924i	12.969 + 4.499i
28	15.277+ 7.658i	22.564 + 10.091i	27.271 + 9.215i	30.552 + 10.637i	18.07 + 7.827i	14.461 + 6.257i	13.077 + 4.727i	10.82 + 3.928i
29	4.607 + 0.581i	4.67 + 0.625i	19.347 + 10.328i	20.466 + 10.856i	9.863 + 3.539i	9.086 + 3.213i	11.225 + 2.869i	10.344 + 2.653i
30	8.346 + 6.4i	14.203+ 9.914i	8.633+ 3.622i	12.045 + 4.885i	11.103 + 5.747i	13.949 + 7.158i	18.511 + 12.295i	15.733 + 10.503i
31	24.697 + 7.107i	29.194 + 9.59i	20.991 + 15.081i	25.903 + 18.273i	12.18 + 7.538i	15.911 + 9.64i	15.352 + 10.031i	15.472 + 10.009i
32	11.052 + 5.936i	12.085 + 6.852i	7.795 + 5.588i	9.822+ 7.104i	8.524 + 7.581i	10.949 + 9.622i	15.509 + 17.348i	14.997 + 17.082i
33	11.229+ 9.870i	10.201 + 8.859i	10.912 + 7.61i	10.341 + 7.263i	15.99 + 12.324i	18.04 + 13.811i	12.497 + 6.681i	11.355 + 6.087i
34	12.624 + 10.256i	16.635 + 12.582i	12.159 + 6.871i	16.249 + 9.397i	9.167 + 7.709i	8.779 + 7.353i	12.506 + 10.108i	14.724 + 11.700i
35	16.947 + 15.598i	16.667 + 15.624i	12.64 + 11.863i	15.204 + 14.047i	21.757 + 12.333i	20.533 + 11.468i	10.383 + 6.926i	12.176 + 8.019i
36	32.484 + 26.185i	25.283 + 20.518i	13.777+ 8.381i	12.818 + 7.866i	19.744 + 20.524i	19.178 + 20.04i	9.927 + 9.293i	9.8 + 9.245i
37	4.075 + 8.204i	6.349 + 10.332i	17.851 + 21.048i	18.325 + 20.934i	12.373+ 14.149i	14.157 + 15.954i	11.663 + 10.574i	11.788 + 10.541i
38	34.214 + 36.399i	33.25 + 36.369i	23.739 + 18.904i	19.016 + 15.411i	16.224 + 16.804i	13.895 + 14.122i	6.883 + 8.479i	6.907 + 8.547i
39	7.254 + 9.371i	11.369 + 13.324i	5.572 + 6.419i	6.91 + 7.784i	9.671 + 12.483i	11.252 + 14.102i	9.540 + 9.296i	7.859 + 7.802i
40	12.559 + 13.824i	11.819 + 13.197i	6.063 + 8.869i	8.651 + 11.235i	13.652\+ 18.457i	13.395 + 18.173i	7.473 + 8.964i	9.203 + 10.689i
41	21.463 + 7.249i	12.953 + 4.483i	9.755 - 0.283i	10.104 - 0.196i	15.955 + 1.539i	18.661 + 1.858i	15.735 + 2.708i	12.504 + 2.09i
42	8.438 + 0.146i	6.406 - 0.124i	9.288 + 1.505i	7.08 + 0.983i	19.845 + 1.696i	20.299 + 1.721i	18.348 + 1.891i	15.111 + 1.5i
43	7.603 + 3.689i	4.61 + 2.379i	11.578 + 2.533i	9.584 + 1.967i	15.561 + 2.384i	12.521 + 1.785i	14.869 + 2.879i	17.887 + 3.455i
44	8.773 + 0.423i	15.608 + 1.869i	26.626 + 3.377i	25.691 + 3.736i	12.955 + 3.917i	13.873 + 4.239i	12.769 + 1.14i	10.635 + 0.911i
45	10.766 + 8.621i	5.003 + 4.505i	17.492 + 9.986i	12.27 + 7.257i	16.155 + 4.857i	14.101 + 4.275i	13.327 + 4.256i	15.831 + 4.904i
46	38.311 + 3.597i	35.298 + 3.567i	15.146 + 5.828i	14.775 + 5.479i	11.664 + 5.297i	11.285 + 5.02i	17.153 + 8.286i	15.091 + 7.309i
47	28.193 + 0.742i	27.961+ 0.926i	11.145 + 3.596i	16.617 + 5.298i	21.342 + 7.507i	23.598 + 8.005i	11.132 + 3.781i	12.702 + 4.29i
48	34.976 + 15.914i	38.79 + 18.18i	20.322 + 13.656i	15.281 + 10.519i	14.007 + 4.598i	10.354+ 3.371i	11.700+ 5.359i	13.529 + 6.097i
49	19.447 + 1.429i	26.597 + 3.017i	10.73 + 5.093i	8.835 + 4.229i	9.148 + 5.461i	10.995 + 6.551i	13.984 + 6.531i	14.747 + 6.812i
50	16.368 + 10.937i	9.516 + 6.713i	19.346 + 7.883i	26.019 + 10.913i	11.921 + 7.774i	8.943 + 6.03i	20.434 + 14.048i	20.608 + 14.029i
51	21.601 + 11.795i	21.976 + 12.085i	14.973 + 5.663i	20.864 + 7.924i	15.157 + 9.206i	14.082 + 8.669i	14.988 + 7.741i	12.368 + 6.561i
52	14.614 + 8.361i	14.208 + 8.073i	17.636 + 14.66i	18.77 + 15.185i	11.163 + 7.491i	11.122 + 7.589i	12.530+ 14.921i	12.751 + 15.176i
53	32.211 + 14.233i	25.412 + 11.883i	11.329 + 10.193i	12.179 + 10.934i	11.862 + 8.907i	12.625 + 9.376i	13.864 + 7.49i	16.641 + 8.8i
54	15.023 + 5.932i	10.624 + 4.21i	14.806 + 9.84i	19.605 + 12.795i	7.023+ 5.911i	9.08 + 7.454i	8.992 + 10.925i	10.087 + 12.074i
55	13.040 + 14.931i	7.349 + 9.003i	8.366 + 10.842i	11.687 + 14.322i	7.422+ 4.101i	8.673 + 4.747i	8.317 + 7.374i	7.083 + 6.485i
56	19.298+ 18.675i	10.764 + 11.358i	9.051 + 9.26i	8.92 + 9.368i	12.19 + 12.088i	10.594 + 10.621i	8.624 + 11.031i	7.685 + 10.036i
57	23.517 + 19.483i	22.162 + 18.503i	26.783 + 24.121i	27.116 + 24.239i	9.045 + 9.977i	6.927 + 8.040i	6.05 + 6.019i	6.522 + 6.421i
58	26.150+ 16.821i	16.843 + 11.09i	15.722 + 17.286i	13.302 + 15.012i	10.227 + 10.024i	9.481 + 9.302i	13.781 + 12.895i	12.620+ 11.848i
59	5.28 + 6.705i	3.934 + 5.621i	9.963 + 13.1361i	8.349 + 11.542i	9.441 + 12.747i	8.127 + 11.24i	12.377 + 9.196i	10.51 + 7.928i
60	7.624+ 14.215i	6.793 + 13.756i	7.146 + 9.72i	5.536 + 8.158i	15.812 + 15.922i	18.165 + 18.42i	10.583 + 13.614i	9.662 + 12.645i
61	14.303 - 1.232i	17.232 - 0.633i	14.319 + 6.552i	9.973 + 4.614i	11.731 + 1.207i	14.904 + 1.79i	14.223 + 0.757i	13.642 + 0.642i
62	6.952 + 0.159i	10.261 + 0.848i	7.324 + 4.169i	7.264 + 4.107i	28.769+ 7.916i	26.935+ 7.558i	24.061 + 4.1i	23.907 + 4.033i
63	9.121 + 2.573i	8.354 + 2.469i	5.841 + 1.062i	6.491 + 1.226i	20.163 + 8.322i	18.396 + 7.407i	9.528 + 1.004i	9.551 + 1.071i
64	7.438 + 3.288i	11.768 + 5.046i	18.387 + 4.671i	13.187 + 3.514i	17.218 + 4.709i	20.947 + 5.661i	18.391+ 4.165i	21.266 + 4.864i

Table 4-13 Codebooks for main diagonal (3×1 vector) under time-varying channel environment

	Codewords for 5 km/hr			Codewords for 15 km/hr			Codewords for 30 km/hr			Codewords for 50 km/hr		
1	9.13	13.23	21.27	15.39	13.12	12.17	15.03	11.46	9.99	14.7	15.66	14.91
2	7.62	6.1	6.61	16.35	18.6	17.11	31.42	32.92	27.78	28.11	26.05	20.92
3	17.95	11.01	8.09	13.26	16.03	19.34	23.11	21.82	18.84	23.26	24.74	23.44
4	40.26	27.29	15.14	21.5	18.26	14.5	21.22	19.06	16.51	13.35	15.33	17.86
5	18.81	21.99	23.09	15.85	21.25	25.46	18.16	18.57	19.16	16.82	19.41	21.34
6	13.9	12.61	10.55	34.22	34.68	28.52	19.95	21.1	19.91	25.85	21.39	16.64
7	12.65	8.27	6.99	38.15	30.54	19.58	9.52	10.51	13.47	19.88	18.53	16.58
8	13.3	24.72	38.65	29.83	28.68	22.82	23.12	17.58	13.2	11.06	10.09	10.82
9	11.2	18.37	28.98	43.49	47.02	36.87	12.53	11.44	11.96	10.51	11.31	13.89
10	7.64	10.41	15.87	20.63	14.28	10.66	17.61	20.83	23.08	15.64	14.01	12.79
11	21.38	34.49	43.23	11.72	16.51	24.05	11.78	12.86	14.83	19.44	16.62	14.21
12	30.47	26.29	18.22	20.07	22.68	22.27	17.83	18.1	16.13	19.29	24.36	26.81
13	17.95	15.18	12.56	8.6	9.43	12.87	10.49	12.9	17.83	13.19	16.82	21.41
14	51.83	54.91	42.13	12.24	10.88	10.78	10.28	9.16	9.7	18.18	16.58	17.57
15	29.08	47.58	56.28	16.14	11.08	8.88	22.46	28.99	32.49	13.14	12.41	12.93
16	25.72	32.98	32.96	17.89	15.46	17.34	18.2	23.96	28.18	15.62	15.73	17.02
17	48.66	39.42	23.32	16.44	18.93	21.33	25.1	24.56	21.15	14.76	13.63	15.17
18	13.16	18.58	22.36	30.65	23.95	16.6	21.05	23.64	23.44	11.1	13.45	17.79
19	12.42	11.09	14.25	9.75	7.94	8.5	14.89	17.3	18.11	15.33	17.49	19.07
20	23.51	23.08	18.15	14.6	22.93	31.49	24.9	27.08	26.08	16.99	17.71	15.97
21	34.8	33.6	25.14	17.85	16.05	13.51	15.87	15.66	14.86	22.56	17.81	13.71
22	24.19	14.06	8.79	14.04	14.73	15.34	19.65	14.12	10.89	17.88	19	18.78
23	30.88	19.69	11.5	20.32	25.62	27.42	30.2	26.76	20.23	23.24	22.55	19.89
24	23.22	18.41	13.66	24.62	22.07	17.76	16.51	14.08	12.35	12.36	13.62	15.26
25	16.05	14.78	18.47	20.89	30.11	35.28	19.28	16.17	14.1	19.78	22.08	22.64
26	25.1	27.78	25.01	20.36	19.9	18.39	13.39	14.83	16.79	20.03	20.56	19.6
27	17.74	19.4	17.05	26.47	18.54	12.74	15.29	18.55	21.26	17.24	15.33	14.58
28	17.48	25.27	29.59	25.97	29.9	28.32	26.67	21.57	15.9	18.55	14.3	11.62
29	6.64	7.25	11.13	24.81	24.99	22.53	14.21	13.41	13.75	14.72	11.97	10.7
30	9.79	9.88	10.55	10.03	12.77	18.19	12.37	15.95	20.82	22.14	20.05	17.04
31	36.86	42.83	35.52	28.7	37.43	37.26	13.81	19.38	25.73	16.12	20.38	24.4
32	12.11	15.4	15.76	11.75	12.12	14.38	17.11	15.32	17.57	25.88	29.22	27.77

The above codebooks can verify our point of view that for the main diagonals, the magnitude of codewords is largest while the magnitude of top off-diagonal entries is smallest. Using the above self-trained codebooks, **Fig. 4-9** and **Fig. 4-11**, demonstrate the effectiveness of the proposed scheme. The first one, **Fig. 4-9**, which is under the time-invariant channel environment, shows that our proposed scheme can attain a smaller MSE even when the number of quantization bits is 4.67 bits, which is much smaller than 14.4 bits.

For diagonal-wise full vector quantization, it is observed that when the velocity is higher, the MSE is smaller. The reason is that mobile users with higher speed would experience more variations in a time slot. On the other hand, in the same time slot, the low speed mobile users experience fewer variations relative to high speed users. **Fig. 4-10** illustrates a simple example to explain the above-mentioned situation. So, when we average the spatial correlation matrix over a certain time slot, the average matrix would be closer to the ensemble average for high speed users, that is, the diagonal-wisely uniform magnitude property for the spatial correlation matrix is more significant. This can explain why a higher velocity results in a smaller MSE.

As for entry-wise differential SQ, the MSE remains roughly the same for all the velocities. Since the differential quantization takes the advantage of the temporal correlation of the channel, lower speed mobile users should have better performance. But, as mentioned earlier, the average spatial correlation matrix is closer to the ensemble average at high speed. So, the difference between $\mathbf{R}_n$ and $\mathbf{R}_{n-1}$ would be smaller. Therefore, at a low velocity, a smaller difference between $\mathbf{R}_n$ and $\mathbf{R}_{n-1}$ results from the temporal correlation of channel, while at a high velocity, it results from the closeness to the ensemble average for every $\mathbf{R}_n$.

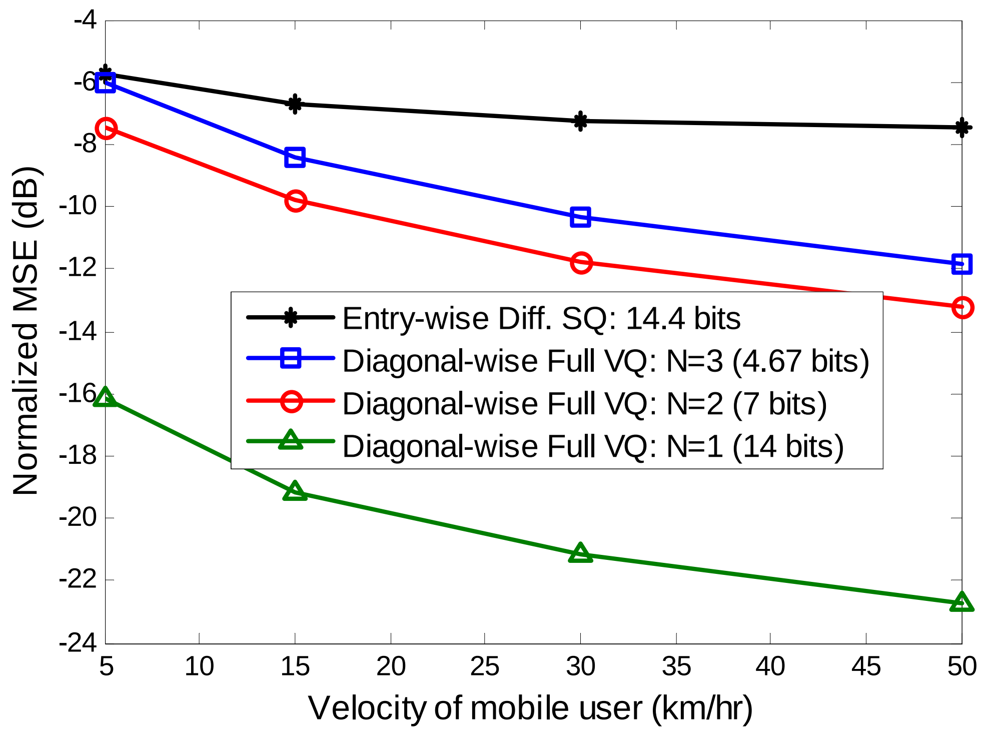

Fig. 4-9 Different number of quantization bits for diagonal-wise full VQ

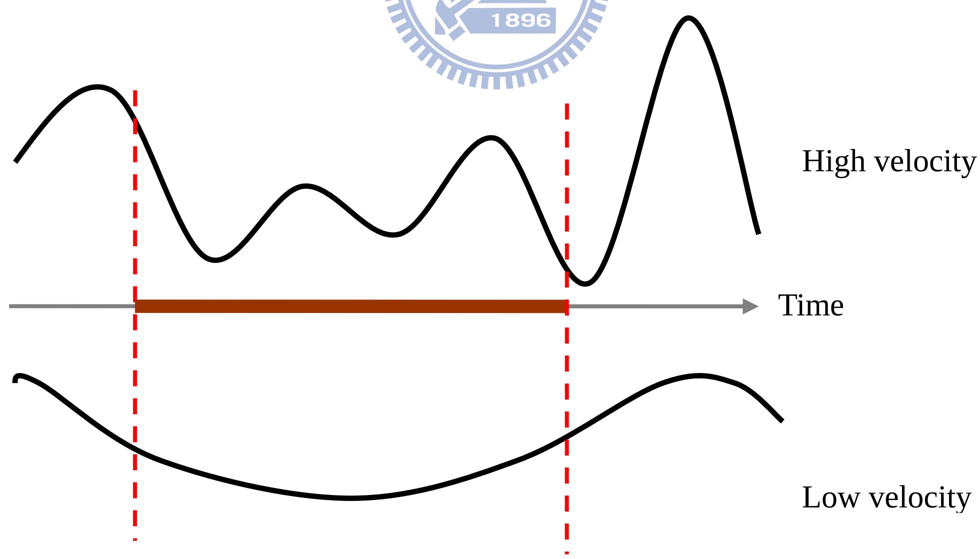

Fig. 4-10 Channel variation for high and low velocities

Fig. 4-11 shows the simulation results for time-varying channel environments (solid lines). We can see that our proposed diagonal-wise full VQ is still effective under time-varying channel environments compared to the entry-wise differential SQ. Also, we can observe that, the MSE under time-varying channel (solid lines) environments is larger than that under time-invariant channel environments (dash lines). The reason is that the range of database for codebook training would be larger under time-varying channel environment, and hence the same size of codebook cannot precisely represents the whole database as in the time-invariant channel environment.

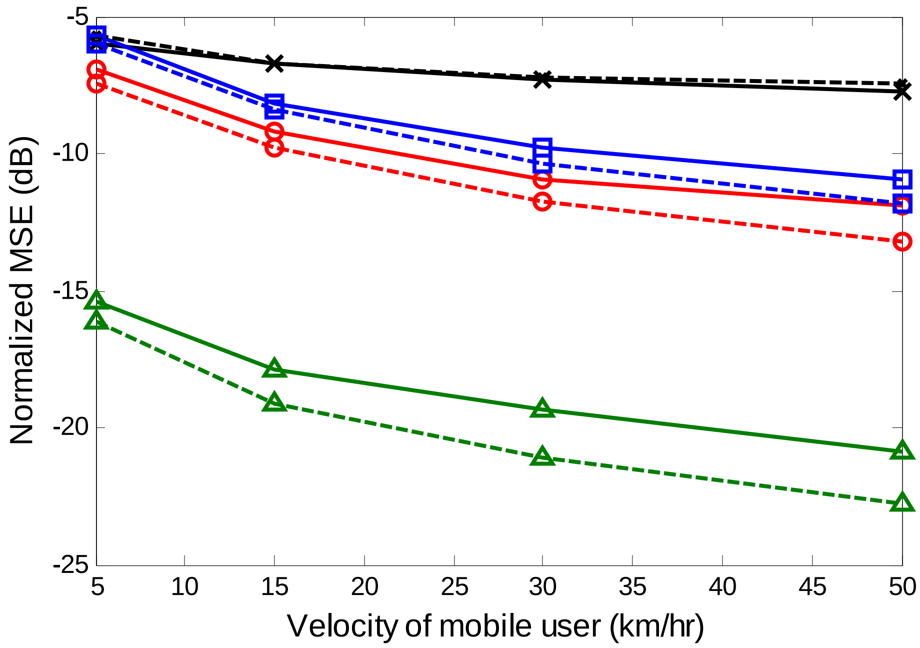

Fig. 4-11 Comparisons of the results with time-varying (solid lines) and time-invariant (dash lines) channel (Legend is as follows)

4.3 Summary

In this chapter, we address the issue of different feedback overheads for different users. From the geometrical point of view, we analyze the interferences and the precoding gain of users with a higher feedback overhead and users with a normal feedback overhead. The simulation results and the geometrical analysis show that the interferences and precoding gain of one specific user mainly depend on its own quantization angular error and independent of other users.'

Also, in this chapter, we propose diagonal-wise full vector quantization and show that it effectively quantizes the spatial correlation matrix with a lower cost of quantization bit. Under time-varying channel environments, the proposed scheme is still superior to the entry-wise differential scalar quantization method although its performance degrades lightly compared to that under the time-invariant environment.

Chapter 5

Conclusion

Limited feedback is a prevailing technique to enhance the system overall performance by relaying back the CSI over a band-limited channel to the transmitter. In this thesis, we focus on reducing the required feedback overhead. In Chapter 2, the multiuser MIMO (each user with single antenna system) with limited feedback is introduced. The temporally correlated channel is simulated by the well-known Jakes' channel simulator. The codebook in LTE Release 8 is also provided. Moreover, we present the commonly used full vector quantization scheme.

In Chapter 3, we propose differential vector quantization scheme to reduce the size of codebook for CSI feedback. The proposed scheme introduces the Predictive Vector Quantization (PVQ) model to perform differential quantization by exploiting the temporal correlation of CSI. Full CSI is periodically fed back using a large number of quantization bits while the remaining differential CSI use fewer quantization bits. The codebook is trained by the well-know GLA with some modifications. The LMMSE predictor is used in the system. Since LTE adopts OFDM as its downlink technique, we further extend the MIMO system to MIMO OFDM system. Also, because the number of subcarriers may be up to 2048 according to [25], it is impossible to feedback all the subcarriers information. Subcarriers are divided into groups and only one subcarrier in each group is fed back to the transmitter. Simulation results show that the proposed differential vector quantization is superior to the conventional full vector quantization in both MIMO and MIMO OFDM systems. The results under different temporally correlated channel environments are also demonstrated and it is shown that our method can successfully reduce the feedback overhead especially at highly correlated channel environments.

However, CSI at transmitter may be not sufficient for the transmitter to determine a suitable precoding matrix. The statistic information such as spatial correlation of the channel can be used to refine the codewords to make the precoding matrix more appropriate in the current communication system. Therefore, in Chapter 4, we propose a diagonal-wise full vector quantization scheme to quantize the spatial correlation matrix. The numerical results show that the proposed scheme can achieve a smaller MSE compared to the entry-wise scalar quantization scheme. Also, in Chapter 4, the scenario of different feedback overheads for different users is considered. We show a simple example to explain the simulation result. From a geometrical point of view, we analyze the interference and precoding gain. Our analysis indicates that under ZF precoding, the lower bound of one user's SINR is only related to the user's quantization angular error and independent of other users'.

The practical limited feedback systems include many problems such as transmission delay, estimation errors at receiver, and non-ideal feedback link. Those problems can be further considered in the proposed methods to make the system more robust. Furthermore, we can investigate its performance under a non-ideal feedback link for the proposed differential vector quantization since the differential quantization scheme is known to be sensitive to the transmission error.

Bibliography

[1] A. B. Gershman and N. D. Sidiropoulos, *Space-time Processing for MIMO Communications*: John Wiley, 2005.

[2] H. Sampath, P. Stoica, and A. Paulraj, "Generalized linear precoder and decoder design for MIMO channels using the weighted MMSE criterion," *IEEE Trans. Comm.*, vol. 49, pp. 2198-2206, Dec. 2001.

[3] V. Mai and A. Paulraj, "Optimal linear precoders for MIMO wireless correlated channels with nonzero mean in space-time coded systems," *IEEE Trans. Signal Processing*, vol. 54, pp. 2318-2332, Jun. 2006.

[4] Z. Xi, D. P. Palomar, and B. Ottersten, "Statistically Robust Design of Linear MIMO Transceivers," *IEEE Trans. Signal Processing*, vol. 56, pp. 3678-3689, Aug. 2008.

[5] H. Weingarten, Y. Steinberg, and S. Shamai, "The Capacity Region of the Gaussian Multiple-Input Multiple-Output Broadcast Channel," *IEEE Trans. Inf. Theory*, vol. 52, pp. 3936-3964, Sep. 2006.

[6] R. W. Heath Jr. and A. Paulraj, "A simple scheme for transmit diversity using partial channel feedback," *Conf. Record of the Thirty-Second Asilomar Conf. on Signals, Systems & Computers*, vol. 2, pp. 1073-1078, Nov. 1998.

[7] A. Narula, M. J. Lopez, M. D. Trott, and G. W. Wornell, "Efficient use of side information in multiple-antenna data transmission over fading channels," *IEEE Journal Select. Areas Comm.*, vol. 16, pp. 1423-1436, Oct. 1998.

[8] Z. Pengcheng, T. Lan, W. Yan, and Y. Xiaohu, "Quantized beamforming with channel prediction - transactions letters," *IEEE Trans. Wireless Comm*, vol. 8, pp. 5377-5382, Nov. 2009.

[9] J. C. Roh and B. D. Rao, "Efficient feedback methods for MIMO channels based on parameterization," *IEEE Trans. on Wireless Comm.*, vol. 6, pp. 282-292, Jan. 2007.

[10] Y. Isukapalli, Z. Jun, and B. D. Rao, "Optimum Codebook Design and Average SEP Loss Analysis of Spatially Independent and Correlated Feedback Based MISO Systems With Rectangular QAM Constellation," *IEEE Trans. Signal Processing*, vol. 57, pp. 2017-2024, May 2009.

[11] J. C. Roh and B. D. Rao, "Transmit beamforming in multiple-antenna systems with finite rate feedback: a VQ-based approach," *IEEE Trans. Inf. Theory*, vol. 52, pp. 1101-1112, Mar. 2006.

[12] N. Zorba, A. Pascual-Iserte, and A. I. P. Neira, "Dynamic bit allocation and differential quantization in feedback link for robust power allocation in multiuser opportunistic beamforming," *IEEE 9th Workshop on SPAWC*, pp. 306-310, Jul. 2008.

[13] S. H. Ting, K. Sakaguchi, and K. Araki, "Differential quantization of eigenmodes for MIMO eigenmode transmission systems," *IEEE Comm. Lett.*, vol. 9, pp. 697-699, Aug. 2005.

[14] M. Trivellato, S. Tomasin, and N. Benvenuto, "On channel quantization and feedback strategies for multiuser MIMO-OFDM downlink systems," *IEEE Trans. Comm.*, vol. 57, pp. 2645-2654, Sep. 2009.

[15] A. Gersho and R. M. Gray, *Vector Quantization and Signal Compression*: Kluwer Academic Pub, 1992.

[16] G. J. Foschini and M. J. Gans, "On limits of wireless communications in a fading environment when using multiple antennas," *Wireless Personal Comm.*, vol. 6, pp. 311-335, Aug. 1998.

[17] W. Santipach and M. L. Honig, "Asymptotic capacity of beamforming with limited feedback," in *Proc. IEEE Int. Sym. Inf. Theory (ISIT)*, pp. 290, 27 Jun.-2 Jul. 2004.

[18] D. J. Love, R. W. Heath Jr, and T. Strohmer, "Grassmannian beamforming for multiple-input multiple-output wireless systems," *IEEE Trans. Inf. Theory*, vol. 49, pp. 2735-2747, Oct. 2003.

[19] N. Jindal, "High SNR analysis of MIMO broadcast channels," in *Proc. IEEE Int. Sym. Inf. Theory (ISIT)*, pp. 2310-2314, Sep. 2005.

[20] K. E. Baddour and N. C. Beaulieu, "Autoregressive modeling for fading channel simulation," *IEEE Trans. Wireless Comm.*, vol. 4, pp. 1650-1662, Jul. 2005.

[21] G. L. Stuber, *Principles of Mobile Communication* 2nd: Kluwer Academic Publishers, 2001.

[22] N. Jindal, "MIMO Broadcast Channels With Finite-Rate Feedback," *IEEE Trans. Inf. Theory,* vol. 52, pp. 5045-5060, Nov. 2006.

[23] A.-Y. Chun Kin and D. J. Love, "On the performance of random vector quantization limited feedback beamforming in a MISO system," *IEEE Trans. Wireless Comm.*, vol. 6, pp. 458-462, Feb. 2007.

[24] K. K. Mukkavilli, A. Sabharwal, E. Erkip, and B. Aazhang, "On beamforming with finite rate feedback in multiple-antenna systems," *IEEE Trans. Inf. Theory,* vol. 49, pp. 2562-2579, Oct. 2003.

[25] 3GPP, TS 36.211,"Evolved Universal terrestrial Radio Access (E-UTRA); Physical Channels and Modulation (Release 8)".

[26] K. Sayood, *Introduction to Data Compression*: Morgan Kaufmann: Morgan Kaufmann, 2000.

[27] S. M. Kay, *Fundamentals of Statistical Signal processing: Estimation Theory*: Prentice Hall, 1993.

[28] IEEE Std. 802.16m/D5, "Part16: Air Interference for Fixed and Mobile Broadband Wireless Access Systems," pp. 603. April, 2010.

[29] R1-101461, "Covariance Matrix Quantization for CSI Feedback," Motorola, Feb. 2010.

[30] "IEEE 802.16m Evaluation Methodology Document (EMD)," Jan. 2009.